

UNIVERSITY OF NAPLES “FEDERICO II”

**DEPARTMENT OF NEUROSCIENCES,
REPRODUCTIVE SCIENCES AND ODONTOSTOMATOLOGY**

PhD Program in Neuroscience – XXVII

Prof. Lucio Annunziato



**CHARCOT-MARIE-TOOTH DISEASE:
INSIGHTS FROM SKIN BIOSPY**

TUTOR

Prof. LUCIO SANTORO

CANDIDATE

Dr. CHIARA PISCIOTTA

1. INTRODUCTION

1.1 Charcot-Marie-Tooth disease

Inherited neuropathies, collectively known as Charcot-Marie-Tooth disease (CMT), are a group of genetically and phenotypically heterogeneous peripheral neuropathies associated with mutations or copy number variations in over 80 distinct genes.¹ Named after the three neurologists who first described the condition in 1886, CMT is the most common inherited neuromuscular disease.² CMT is a motor and sensory neuropathy (HMSN) that is closely related to two other rarer inherited neuropathies: distal hereditary motor neuropathy (dHMN), which has predominantly motor involvement, and hereditary sensory/autonomic neuropathy (HSN or HSAN), which involves only or predominantly sensory and autonomic nerves. These three disorders represent a continuum and are often collectively termed CMT and related disorders.³

CMT is divided into different forms based on the pattern of inheritance and neurophysiological studies. Autosomal dominant forms are subdivided into demyelinating (CMT1) and axonal (CMT2) forms. CMT4 and CMTX designate the autosomal recessive and X-linked forms, respectively.⁴ The term Dejerine-Sottas neuropathy (DSN) is currently used primarily to denote severe early-onset clinical phenotypes regardless of the inheritance pattern.⁵ The classification of CMT has been divided further into subtypes, identified by letters, as defined by the mutated gene (Table 1).

Epidemiology

The prevalence of CMT is about 1 in 2500 people, with a global distribution and no ethnic predisposition. CMT1A, associated with 17p11.2 duplication in the region containing the peripheral myelin protein 22 gene (*PMP22*), is the most common form of CMT and accounts for 60 to 70% of demyelinating CMT patients (around 50% of all CMT cases). Mutations in the gap junction beta 1 gene (*GJB1*) causing CMTX result in approximately 10 to 20% of CMT cases and CMT1B associated with mutations in the myelin protein zero gene (*MPZ*) accounts for less than 5%. Patients with CMT2 are about 20% of all cases. The prevalence of hereditary neuropathy with liability to pressure palsies (HNPP) is not known, but about 85% of patients with clinical evidence of

this syndrome have a chromosome 17p11.2 deletion.⁶ Although there are many genes associated with CMT, mutations in only four genes (*PMP22* duplication/deletion, *GJB1*, *MPZ* plus *MFN2* in Northern Europe and American populations or *GDAP1* in Mediterranean populations) account for over 90% of CMT cases.⁶⁻¹⁰ Mutations in the ganglioside-induced differentiation-associated protein 1 gene (*GDAP1*) lead to both recessive (CMT4A/AR-CMT2K) and dominant (CMT2K) form of CMT. Rarer forms include CMT2E due to mutations in the neurofilament light chain gene (*NEFL*), CMT2B associated with Ras-associated protein RAB7 mutations and CMT2C (TRPV4 gene mutations).¹¹

Clinical Manifestations

Despite phenotypic variability, there are characteristic clinical patterns for many types of CMT (Table 2). The “classical” CMT phenotype consists of normal early milestones such as beginning to walk by a year of age. This is followed by gradually progressing weakness, and sensory loss during the first 2 decades of life. The classic phenotype typically features a steppage gait, pes cavus, sensory loss in a stocking or glove distribution, inverted champagne bottle legs, and atrophy in the hands (Figure 1A, 1B and 1C). Though both motor and sensory nerves are usually affected, the more prominent phenotypic characteristic is related to motor difficulty in most cases. Physical examination shows decreased or absent deep tendon reflexes, often diffusely but always involving the Achilles tendon. Findings are usually symmetric. Pronounced asymmetries in symptoms suggest HNPP if they are episodic. Otherwise they are more consistent with acquired disorders. Patients with classical CMT almost always have impaired proprioception with balance difficulty. Affected children are usually slow runners and have difficulty with activities that require balance (e.g., skating, walking along a log across a stream). Ankle-foot orthotics are frequently required by the third decade. Fine movements of the hands for activities such as turning a key or using buttons and zippers may be impaired, but the hands are rarely as affected as the feet. Deep and superficial muscles that are innervated by the peroneal nerve, such as the tibialis anterior and peroneus brevis and longus muscles often cause more symptoms than do the plantar flexion muscles innervated by the tibial nerve, such as the gastrocnemius. As a result, tripping and spraining one's ankle are frequent

symptoms. Most patients remain ambulatory throughout life and have a normal lifespan.

However, CMT, as well as genetically, may be clinically heterogeneous, with variability in the age of onset, speed of progression and electrophysiological findings. Onset may differ depending on the genetic subtype, including early onset, infantile forms with delayed milestones (historically designated DSN) and late-onset, adult forms. Symptoms are usually slowly progressive, especially for the classic and late-onset phenotype, but can be severe, particularly in early-onset forms.¹²

Electrophysiology

Electrophysiological studies allow for classification of CMT into demyelinating (CMT1) and axonal (CMT2) forms. The standard cut-off for demyelinating motor nerve conduction velocity (MNCV) is 38 m/s in the upper extremities. Axonal forms (CMT2) exhibit MNCVs greater than 45 m/s but a decrease in compound muscle action potential (CMAP) amplitudes. The dominant intermediate forms (I-CMT) show MNCVs between 25-45 m/s. Conduction velocities are performed in the upper limbs because CMAP amplitudes are often unobtainable in the legs, even for demyelinating forms of CMT, due to either conduction failure or secondary axonal degeneration.

The usual electrodiagnostic finding in demyelinated inherited neuropathies is widespread uniform slowing of conduction velocities, as opposed to the multifocal segmental slowing found in demyelinating acquired neuropathies in which temporal dispersion and conduction blocks are frequently seen. Exceptions to this rule are women with CMTX, patients with HNPP and some CMT1B cases with specific *MPZ* mutations. In these cases, focal demyelination with temporal dispersion or conduction block can be seen. In other cases of CMT1 the finding of focal slowing should raise the possibility of a superimposed inflammatory neuropathy.¹³

Pathobiology

A common feature of most genes mutated in CMT is the role they play in maintaining the structure or function of cellular components of the peripheral nervous system, myelinating Schwann cells and the axons they ensheath

(Figure 2). Impaired interactions between axons and mutant Schwann cells seem to be the common process linking all forms of demyelinating CMT. Most cases of CMT1 are caused by mutations in myelin specific genes including *PMP22* (CMT1A), *MPZ* (CMT1B) and *GJB1* (CMT1X), or other genes associated with Schwann cell function, including those that exert transcriptional control of myelination and intracellular trafficking. At a pathological level dysmyelination, demyelination, remyelination, and axonal loss are characteristic features of the various demyelinating forms of CMT1. In DSN, myelin may never have formed normally which is referred to as dysmyelination. In CMT1, onion bulbs of concentric Schwann cell lamellae are usually present on nerve biopsies (Figure 3A and 3B), with loss of both small- and large- diameter myelinated fibers and a decrease in the number of myelinated axons. Focal, sausage-like thickenings of the myelin sheath (tomacula) are characteristic of HNPP but may also be found in other forms of CMT1, particularly CMT1B. In CMT1 disability typically correlates better with secondary axonal degeneration than with demyelination itself, again demonstrating the importance of Schwann cell–axonal interactions in demyelinating disease.¹⁴

Several recent studies have demonstrated a susceptibility of Schwann cells to mutations yielding misfolded proteins, as seen in certain *PMP22* and *MPZ* point mutations.¹⁵⁻¹⁷ Misfolded proteins may accumulate in the endoplasmic reticulum (ER) of Schwann cells inducing a unfolded protein response (UPR); a series of cellular events that help the ER to cope with the increased metabolic demand caused by retention of the misfolded protein. This, in turn, causes down-regulation of the myelination program genes and dedifferentiation of Schwann cells, a toxic gain of function that worsens with the demyelination and is potentially amenable to therapeutic intervention.^{18,19}

Spinal motor neurons and dorsal root ganglion sensory neurons that are affected in CMT have particular challenges in maintaining homeostasis, as their axons extend up to 1 m distal from the cell body. Since the majority of neuronal proteins are synthesized in the cell body, intensive transport of proteins must occur between the soma and the axonal extremity via anterograde transport. Additionally, signals from the periphery containing toxic or pro-survival factors, as well as damaged proteins, return to the cell body via retrograde transport.²⁰ Indeed, axonal trafficking is emerging as a common theme of various seemingly

diverse genes that are associated with CMT type 2. Mutations in genes associated with axonal structure and function result in CMT2. Some examples include mutations in proteins of the neuronal cytoskeleton (NEFL, CMT2E), proteins associated with axonal mitochondrial dynamics (mitofusin 2-MFN2, CMT2A and GDAP1, CMT2K) and protein associated with regulation of membrane and intracellular trafficking (RAB7, CMT2B, for example). The pathological hallmark of CMT2 is axonal degeneration with loss of all types of nerve fibers in the absence of onion-bulb formation.

2. BACKGROUND

2.1 CMT and skin biopsy

The advent of genetic testing has made sural nerve biopsy unnecessary for diagnosing most cases of CMT, particularly because the technique is somewhat invasive. Unfortunately, this has led to an inability to evaluate morphological effects by the various mutations on human nerves. Since animal models do not always faithfully reproduce human pathology the lack of human nerve tissue has limited investigations into pathogenic mechanisms of CMT. Skin biopsies increasingly offer a minimally invasive approach to overcome this problem.

Skin biopsy is commonly performed using a disposable 2-3 mm punch under sterile technique with topical anesthesia. There is no need for suture, and a barely visible scar may remain. It can be performed in any site of the body, on both hairy (shoulder/thigh/leg) and glabrous skin (distal/proximal phalanx of the fingers/fingertips). It is a valid tool for studying the innervation of unmyelinated (C), small myelinated ($A\delta$) and large myelinated ($A\beta$) fibers, after immunohistochemistry (IHC) with antibodies against different components of both the axons and myelin sheath. Specifically, the innervation of autonomic structures can be detected using function-related markers to stain adrenergic, noradrenergic and cholinergic fibers.²¹

Recent studies have shown that the typical morphological changes of myelinated fibers in sural nerve biopsy specimens from patients with CMT can be detected also in dermal nerves, widening the applications of skin biopsy. Beginning with studies of glabrous and hairy skin these biopsies have already

provided pathogenic information in sensory nerves from patients with CMT1A such as reduced Meissner corpuscles (MC) density, shortened internodal length and abnormal paranodal-juxtaparanodal architecture.^{22,23} Moreover, reliable methods for RNA and protein extraction from human skin biopsy specimens have widened this field of research in CMT, giving the opportunity to investigate markers otherwise hardly detectable with IHC.^{24,25} Studies on the molecular architecture of myelinated fibers and gene expression can be helpful in obtaining information on genotype-phenotype correlation and new insight into molecular mechanism of pathology. Following these recent findings, skin biopsy has been used as an outcome measure to assess if treatment with ascorbic acid can modify the expression of PMP22 in patient with CMT1A.²⁵

Regarding other forms of CMT, limited studies on cutaneous innervation are reported and the data are from either single cases or few patients. Moreover, unmyelinated and small myelinated fibers have never been described so far, even in CMT1A where their involvement is anecdotally reported.

2.2 Axonal degeneration in CMT

In the peripheral nervous system, Schwann cells tightly communicate with axons in order to regulate their development, function and maintenance. Schwann cells and axons interact at multiple points along the peripheral nerve, including the adaxonal (opposing the axon) membrane, paranodal myelin loops, microvilli and juxtaparanodal basal lamina. These interactions are mutually beneficial, providing trophic support to the axon and myelinating cues to the Schwann cell. An example of this important interaction is the occurrence of secondary axonal degeneration in all forms of demyelinating CMT. Indeed, although the primary metabolic or structural defect often affects either the myelin or the axon, axonal degeneration represents the final common pathway in both forms of peripheral neuropathies. In demyelinating neuropathies, the secondary axonal degeneration presumably occurs because of inadequate Schwann cell support of the axon. In these neuropathies secondary axonal degeneration may contribute more to clinical impairment than the primary demyelination.²⁶

3. AIM OF THE STUDY

The aim of our project was to study the cutaneous innervation of patients with different subtypes of CMT and investigate the pathomechanisms underlying each form. We have also evaluated the different amount of axonal degeneration in demyelinating and axonal form of CMT. In particular, our work was structured in three parts:

- We evaluated small myelinated and unmyelinated fiber degeneration in patients with the most common demyelinating form of CMT (CMT1A) by quantifying the epidermal nerve fiber (ENF) density and sudomotor, pilomotor, and vasomotor nerves. We compared our morphological results to those from functional studies.²⁷
- We investigated large fiber axonal loss by quantifying MC and intrapapillary myelinated endings (IME) in different CMT subtypes, both demyelinating and axonal. Moreover, we evaluated morphometric changes in myelinated dermal nerves by measuring fiber caliber, internodal and nodal gap length.²⁸
- We studied the expression and assembly of axonal transport proteins (neurofilament and α -tubulin) in a form of axonal CMT (CMT2E), and the effects on fiber caliber and nodal/paranodal regions.²⁹

4. MATERIALS AND METHODS

4.1 Patients

For the study of small fiber involvement 20 unrelated patients (Table 4) (male/female 5/15; mean age 42.9 ± 8.4 years) from 20 kinships with a clinical and genetic diagnosis of CMT1A were included in the study. Patients were also screened to identify and exclude participants with possible alternative causes of involvement of small fibers, such as abnormalities of glucose metabolism, endocrine function, vitamin E, B12 and folic acid deficiency, hepatic or renal failure, HIV, or connective tissue disorders.

For the evaluation of large fiber loss and morphometric analysis in dermal nerves 31 CMT patients were included in the study. Based on molecular genetic analysis the following CMT genotypes were included: CMT1A (n= 10),

CMTX1 (n= 9), late-onset CMT1B (n= 5), CMT2B (n= 3), CMT2C (n=3) and AR-CMT2K (n=1).

Lastly, for the study of the axonal transport we evaluated 9 affected individuals from two generations of a large family with a clinical and genetic diagnosis of CMT2E (Glu396Lys) (Figure 4).

All patients were older than 18 years at the time of enrollment and underwent neurological examination and standard nerve conduction studies. Clinical impairment was assessed using the validated CMT Neuropathy Score (CMTNS).^{30,31} The Institutional Ethics Committee approved the study and a written informed consent was obtained from all participants in the study.

A control population of healthy age- and sex-matched controls was included in the study.

4.2 Skin biopsy

All patients underwent skin biopsies that were processed by either indirect immunofluorescence or electron microscopy (EM) or western blot (WB) analysis.

Immunofluorescence

Skin samples were obtained with 2-mm punch from the fingertip (at the vortex of III finger) or the proximal phalanx of the second finger, and by a 3-mm punch from the thigh and distal leg (union of middle third with the lower third). Specimens were fixed in cold Zamboni solution, cryoprotected in 20% sucrose phosphate-buffered saline (PBS), and cut in 50- μ m-thick sections by means of a sliding microtome. Free-floating sections were incubated overnight with a panel of primary antibodies to mark both myelinated and unmyelinated somatic and autonomic nerve fibers. Secondary antibodies conjugated with cyanine 2 and 3 were used to visualize the structures of interest. ULEX Europaeus agglutinin 1 coupled with cyanine 5 was used to visualize blood vessels and epidermis. Antibody features, source, and dilution are listed in table 3.

Quantification of cutaneous nerves - Somatic nerves

ENF density (number per linear mm) was calculated on 4 sections double-stained with protein gene product (PGP) 9.5 and collagen IV (Col IV)

according to standard criteria.²¹ A qualitative evaluation of peptidergic nerve fiber populations was performed on 2 sections for each biopsy marked with substance P (SubP) and calcitonin gene-related peptide (CGRP).

Quantification of Meissner corpuscles and intrapapillary myelinated endings was performed in glabrous skin samples. Density values (numbers of structures per square millimeter) were obtained following previously described procedures.³² Receptors whose morphology appeared completely disrupted with loss of their coiled shape in PGP stained sections were considered atrophic and therefore were not included in the count.

Quantification of cutaneous nerves - Autonomic nerves

A qualitative evaluation of sudomotor, pilomotor, and vasomotor nerves was performed in all skin samples using the pan-neuronal marker PGP and selective cholinergic and noradrenergic markers vasoactive intestinal peptide (VIP) and dopamine b-hydroxylase (D β H).^{33,34} A quantitative assessment of sudomotor nerves in skin samples from the leg from 10 subjects (P1 to P10) was also performed. For this purpose, using a non-laser confocal microscope (AxioImagerM2 with Apotome2, Zeiss, Jena, Germany), 3D digital images of sweat glands were acquired using a 203 objective (Zeiss EC Plan NeoFluar 203/0.5). To avoid non representative sweat gland fragments, only sweat glands at least 25 μ m thick were included in quantifications. The total length of sudomotor nerves immunoreactive for PGP and VIP was calculated using the nerve tracing module Autoneuron, a part of Neurolucida software (Microbrightfield Bioscience, Williston, VT). This enabled us to trace nerve fibers through 2- μ m optical sections of confocal z-stacks. Sweat gland volumes were calculated by manually tracing the outside contour on alternate optical sections of composite confocal images showing PGP 9.5 or VIP with Col IV and ULEX. A value of nerve density per gland volume (nm/ μ m³) was obtained. This method of quantification was previously validated by comparison with an unbiased estimation of sudomotor nerve total length by stereologic measures.³⁵

Morphometric analysis of myelinated nerve fibers

3D digital images of all myelinated fibers present in 3 PGP/myelin basic protein (MBP) double stained sections were acquired using confocal

microscopy (Zeiss Apotome2) and a 20x objective for the measurements of calibre, internode and nodal gap length (Figure 5A). Internodal and nodal gap lengths were measured on the stack of z-series images using Neurolucida or Image J software (NIH, Bethesda, MD, USA). Nodal gap was measured as the length of the fiber not marked by MBP (Figure 5B₁ and 5B₂) and it included nodal and part of paranodal regions. The measurement of internodal length was performed only when 2 consecutive nodes were identified by tracing the internode on the Z-stack of confocal images (figure 5B₃). Four calibre measurements for each internode (Figure 5B₄) were obtained and a mean value was reported.^{32,36} The Pan-Neurofascin/MBP double stained sections (1 section for each biopsy) (Figure 5C and 5D₁) were used to verify that all the myelin gaps along the fibre course corresponded to nodes and to qualitatively evaluate the nodal/paranodal region.

Fluorescence quantification

For the fluorescence quantification parameters including pinhole size, detector gain, amplifier offset, amplifier gain and laser intensity were first set for normal control tissue, and the same setting used for all samples imaged on a given day.³⁷ Both control and patient sample images were obtained at the same day after the staining. For each sample five non-overlapping sections were acquired. Image analysis was performed using Image J software (NIH, Bethesda, MD, USA). Fluorescence intensity was measured for both NF-L (neurofilament-light) and PGP 9.5 at the same time, choosing an intensity threshold in the PGP channel so that only the axons were highlighted, corresponding to our regions of interest on both PGP and NF-L channel. Then we calculate the NF-L/PGP ratio in order to obtain a relative value of NF-L intensity over the PGP-stained axons and rule out a possible role of nerve fiber loss in reduced NF-L staining. Alpha-tubulin fluorescence intensity was evaluated as well.

Electron microscopy

Skin samples for EM study were obtained by a 2.5 mm punch from the volar aspect of the forearm. Specimens were fixed in 2.5% glutaraldehyde solution overnight, then washed in PBS three times for 10 min, osmicated for

1.5 hours, dehydrated and embedded in Epon. The semithin sections (1 μm thickness) were stained with Toluidine blue and examined under a light microscope. The ultrathin sections were contrasted with lead citrate and uranyl acetate and examined under EM (Transmission Electron Microscope, JEOL 1230).

Western blot analysis

Skin samples for WB analysis were obtained by a 3.5 mm punch from the shoulder and immediately frozen in liquid nitrogen. Snap frozen samples were then pulverized, dissolved in lysis buffer (Radioimmunoprecipitation assay (RIPA) buffer, Sigma R0278 and proteinase inhibitors), kept on ice for at least 30 min and centrifuged at 14000 g for 10 min at 4°C. The protein content of the supernatant was determined using a bovine serum albumin standard curve. Equal amounts of the protein were loaded on 10% sodium dodecyl sulfate (SDS)-polyacrylamide gel electrophoresis (PAGE) gels, and electroblotted onto polyvinyl difluoride membranes. The primary antibodies used are listed in table 3. Horseradish peroxidase-conjugated secondary antibodies (1:5,000-1:20,000 dilution; Sigma) were detected using enhanced chemiluminescence (ECL) reagents (Amersham ECL Prime Western Blotting Detection Reagent, RPN 2232) with autoradiography film (Kodak Scientific Imaging Film, Blue XB). Results were normalized for α -tubulin and the control sample signal was used as the reference. Moreover, the signal density was calculated by Image J software (NIH, Bethesda, MD, USA), the ratio NF-L/ α -tubulin was obtained for both patients and control, and any value less than the control value was considered abnormal.

4.3 Functional studies

Small Fiber Neuropathy Symptoms Inventory Questionnaire

For the study of small fiber involvement all CMT1A patients completed the Small Fiber Neuropathy Symptoms Inventory Questionnaire (SFN-SIQ).³⁸ A subgroup of 10 patients (P1 to P10) underwent an additional extensive protocol to assess autonomic and sensory function. To avoid interferences from stress or fatigue with the results of psychophysical QST and the cardiovascular

autonomic nervous system testing, the evaluations were performed on 3 separate days according to the following schedule: CVRs on day 1, DST and SSR on day 2, and QST (tactile and thermal thresholds, and mechanical pain perception) on day 3.

The 13-item SFN-SIQ questionnaire was used to provide data on clinical symptoms of small nerve fiber impairment. Patients were questioned on the occurrence of autonomic and sensory symptoms in their daily life. For each item, patients were assigned a score based on occurrence of the symptom: 0= never; 1= sometimes; 2= often; 3= always. The scoring ranges from 0 (no symptoms) to 39 (all symptoms are always present).

Quantitative sensory testing

Quantitative sensory testing (QST) was performed on the dorsum of right hand and foot for 6 sensory modalities (tactile threshold, thresholds to warm and cold innocuous and noxious stimuli, mechanical pain perception) as previously described.³⁹

Dynamic sweat test

Postganglionic sudomotor function was evaluated using the dynamic sweat test (DST). Briefly, after stimulation with 1% pilocarpine by iontophoresis (5 minutes at 2 mA) on the lateral aspect of distal leg (union of middle third with the lower third), sweating output, visualized with colorimetric method, was recorded using a video camera. Activated sweat gland density per cm² and sweat volume per gland and per cm² were calculated analyzing sweat drop imprints on seriate frames from digital recording.⁴⁰

Sympathetic skin response

Sympathetic skin response (SSR) was recorded at hands and feet after random single 1-ms stimuli at the wrist, using surface electrodes; a bandpass of 0.2–100 Hz was used. The skin temperature was maintained between 32 and 34°C.

Cardiovascular reflexes

To assess cardiovascular reflexes (CVR), the following tests were performed: heart rate variability at rest and during deep breathing, Valsalva ratio, 30/15 ratio, and blood pressure changes to standing and to handgrip.⁴¹

4.4 Statistical analysis

Statistical analysis was performed using STATA 12.1 for Windows (StataCorp LP, USA). The ANOVA test with the Bonferroni post hoc test for parametric variables or the Kruskal-Wallis test for non-parametric variables were used. For two group comparison, Student t test for unpaired data and Mann-Whitney U-test (when analyzing nonparametric data) were used to compare skin biopsy findings from patients and controls. The Spearman rank-order correlation test was used to investigate the correlations between non parametric variables. The Robust test of equality of variance was used for verifying the homogeneity of data between groups. A p-value of <0.05 was considered significant.

5. RESULTS

5.1 Patients

Disease severity, as determined by the CMTNS, ranged from mild to severe impairment (scores between 2 and 30). Individual scores along with additional clinical information about the patients are provided in table 4, table 7 and table 8.

5.2 Small fiber involvement in CMT1A

Skin biopsy findings

Our findings demonstrated a loss of somatic and autonomic nerve fibers in the distal leg and fingertip while cutaneous innervation from the thigh was relatively spared (Figure 6). Quantitative assessment of ENF, MC, and IME are summarized in table 5. ENF density in fingertip (Figure 6A and 6B) and leg (Figure 6E and 6F) was lower ($p < 0.001$) in patients compared to controls, supporting a length-dependent small fiber neuropathy. A loss of MC and IME

(Figure 6A and 6B) was also found ($p < 0.001$). In our patients the loss of ENF at distal leg correlated with the increase in heat-pain thresholds ($p < 0.05$) and with tactile thresholds ($p < 0.05$). No ENF density differences were found between patients with and without burning pain. Peptidergic (SubP and CGRP immunoreactive) fibers appeared poorly represented in skin samples of patients compared to controls. All dermal adnexa showed aspects of derangement of nerve supply with involvement of sudomotor (Figure 7A and 7B), vasomotor (Figure 7C and 7D), and pilomotor (Figure 7E and 7F) fibers. The most frequently observed morphologic abnormalities were nerve thickening, a chaotic distribution of nerve fibers around dermal annexes, and a loss of the regular coiling around tubules or vessels. Quantitative evaluation of sudomotor innervation was performed on a total of 195 sweat glands (65 from patients and 130 from controls, 87 with PGP and 108 with VIP). The density of sudomotor nerves was lower ($p < 0.001$) compared to normal healthy controls using both the pan-neuronal marker PGP and the selective cholinergic marker VIP (Table 6) and correlated ($p < 0.001$) with the density of activated sweat gland density (figure 8A). Eighty percent of patients had a sudomotor innervation below 5% cut-off evaluating PGP-immunoreactive fibers and 90% evaluating VIP-immunoreactive fibers. The loss of MC correlated with the increase in tactile thresholds and with the loss of ENF in the same site. The loss of ENF from distal leg correlated with the loss of sudomotor nerve fibers from the same site ($p < 0.05$), suggesting a parallel involvement of unmyelinated autonomic and somatic nerve fiber populations. Activated sweat gland density after pilocarpine stimulation correlated with sudomotor innervation as well as with ENF ($p < 0.01$) and MC loss ($p < 0.05$).

Functional studies

At the SFN-SIQ all patients reported at least 2 symptoms related to dysfunction of small nerve fibers (Table 6). Sweating disorders (hypohidrosis/hyperhidrosis) (60%), palpitations (50%), and gastrointestinal complaints (50%) were most frequently reported. Burning feet occurred in 6 out of 20 patients.

For the QST, the mean values of sensory thresholds for all modalities were higher ($p < 0.01$) than those in controls (Table 6). All patients but one had

increased thresholds in sensory modalities involving both C and A- δ fibers, as well as an increase in A- β -fiber-related tactile thresholds. Abnormalities in the feet were greater than those in the hands. None of the patients showed thermal hyperalgesia.

At the DST, patients had a marked reduction of both density of activated sweat glands and mean sweat output for each gland ($p < 0.001$) (Table 6). Hypohidrosis (sweat output/cm² less than 5^o percentile cut-off) was present in 7 of the 10 patients analyzed.

The SSR was obtained in all patients in both hands and feet. The amplitude of SSR recorded at feet was lower in patients than in age- and sex-matched controls ($p < 0.05$) (Table 6).

At the CVR study, only 1 patient showed a cardiac dysautonomia, with abnormalities in 2 tests (30/15 ratio and blood pressure changes to standing), while 2 patients showed borderline results with abnormalities in only 1 test (30/15 ratio) (Table 6).

The loss of ENF in all the 3 sites, as well as the sensory thresholds, the loss of sudomotor nerves, and the deficit in sweating output increased with age. The age effect appeared particularly evident on the loss of leg ENF; the age-disease interaction was significant ($p = 0.04$) for this parameter in a model of multiple linear regression (Figure 8B).

5.3 Large fiber investigation in different CMT subtypes

Morphological analysis

All patients from each CMT genotype had a significant loss ($p < 0.005$) of MC and IME compared to healthy controls (Table 7). The axonal group as whole tended to have a greater loss of MC and IME than CMT1A and this was especially evident in CMT2C group and in AR-CMT2K patient who presented a complete loss of MC and IME (Table 7). No correlations with disease severity was found in any CMT subtypes. In addition to the nerve fibre loss, several aspects of nerve degeneration were present. MC showed abnormalities in their shape (Figure 9B and 9C compared to 9A) and in their position (located at the base instead of the apex of the dermal papillae).

Morphometric analysis

Our findings showed a significant difference in both internodal and nodal gap length among the seven groups ($p=0.0001$). The two group comparison showed that each CMT genotype had shorter internode ($p<0.009$) and longer nodal gap ($p<0.0001$) compared to healthy controls (table 7). CMT1A had significantly shorter internodes ($p<0.001$) and longer nodal gaps ($p<0.001$) than the axonal CMT group. Moreover, CMT1A patients had significantly ($p<0.05$) longer nodal gaps than any other CMT genotype. No difference was evident within the axonal group between patients harbouring mutations in myelin genes (i.e. *MPZ*, *GJB1*) and those with mutations in axonal genes (i.e. *RAB7*, *TRPV4* and *GDAP1*). The variability around the mean internodal length was comparable between each CMT genotype and controls suggesting that the reduction in internodal length observed in each CMT genotype affected nerve fibres uniformly (Figure 10). Fiber calibre was not different among CMT genotypes and between each CMT genotype and controls. Myelinated fibres showed large variability in the calibre, fragmentation (Figure 9D) and swellings (Figure 9E and 9F). Neurofascin/MBP double staining showed asymmetrical distribution (Figure 9H and 9I) of paranodes compared to control (Figure 9G).

Finally, although segmental demyelination and subsequent remyelination may be a pathological feature in sural nerve biopsies from CMT1A we identified no segmental demyelination in any of internodes from CMT1A patients. These data are in keeping with those previously reported in CMT1A patients by Saporta et al.²³

5.4 Study of the axonal transport proteins in CMT2E

Immunofluorescence and Western blot analysis

We performed immunohistochemistry on myelinated dermal nerves from patients and controls. Results from controls demonstrated many axons labeled by the axonal marker PGP 9.5 and with antibodies to NF-L (Figure 11A I, II). Alternatively, axons from patients were not labeled with antibodies to NF-L but were labeled by PGP (Figure 11A IV, V). In order to measure the difference between controls and patients we quantified the fluorescence intensity in the two groups. The analysis demonstrated a lower NF/PGP ratio in patients than

controls ($p < 0.01$) (Figure 11B). There was no correlation between NF-L levels and clinical severity as measured by the CMTNSv2 ($p = \text{NS}$). We then labeled axons with antibodies to α -tubulin to determine whether the transport of other molecules such as α -tubulin was affected by the mutation. Many axons in both patients and controls were labeled with α -tubulin and no difference in staining intensity was detectable between the two groups. In addition, many axons from patients but not controls were labeled with α -tubulin but not with NF-L (Figure 11A III, VI). We concluded that the decreased NF-L immunolabeling was not a consequence of axonal degeneration but rather was a specific consequence of the NF-L mutation. Results from WB analysis confirmed these data as NF-L expression was decreased in patients with a complete absence of NF-L band in two of them, while α -tubulin expression was normal (Figure 11C). The ratio NF-L/ α -tubulin was markedly reduced in patients (Figure 11D).

Electron microscopy

In order to investigate NF accumulation, we also evaluated dermal nerves from our patients by electron microscopy (Figure 12A). No abnormalities of myelin sheaths were observed on either semi-thin or EM sections. Many Schwann cells without axons (bands of Bungner) were present, suggesting prior axonal degeneration. No aggregates were observed. Our results were similar to what was previously reported in sural nerve biopsies from CMT2E patients with Glu396Lys.^{42,43}

As the aggregates were made up of phosphorylated NF in the mutant mouse,⁴⁴ we performed additional staining with antibodies to phosphorylated NF at HIC but again we did not detect any aggregate formation (data not shown).

Furthermore, previous studies showed that the distribution of mitochondria was altered in cultured cells with aggregated NF due to expression of CMT-causing NEFL mutants.⁴⁵ In our patients mitochondria were distributed normally into the axons and neither their shape nor their number was affected by NF disruption.

Morphometric analysis

Prior studies have demonstrated a close correlation between the number of NF and the diameter of myelinated axons in the peripheral nervous

system.^{46,47} To determine whether the reduction of NF-L effected the caliber of axons in our patients we performed a morphometric analysis on the dermal nerves from our patients and controls. Our results demonstrated smaller axonal calibers in patients compared to controls ($p < 0.01$) (Figure 12B), providing further evidence of the NF role in the maintenance of the axonal diameter and supporting the feasibility of evaluating dermal nerves to address this question.

Study of the nodal and paranodal regions

A previous study of nodal architecture in NF deficient mouse showed normal placement, organization, and physical dimensions of nodes of Ranvier.⁴⁸ Our results demonstrated that sodium channels and Caspr are correctly localized in CMT2E patients (Figure 13), confirming that, despite the axonal NF deficiency, the molecular architecture of nodal and paranodal regions is not impaired in CMT2E. This observation supports the hypothesis that NF, as cytoskeletal components of the internodal domain of axons, are not required to position nodal and paranodal molecules.

6. DISCUSSION

6.1 Small fiber involvement in CMT1A

Our results demonstrated length dependent small fiber abnormalities in all patients with CMT1A. Specifically, morphologic studies revealed a length-dependent decrease in ENF density that correlated with functional measures of small fiber somatic and autonomic functions such as QST, reduced numbers of activated sweat glands, and decreased numbers of sudomotor nerve fibers. Thus, small nerve fiber abnormalities are clearly present in patients with CMT1A.

Somatic nerves

Sensory symptoms in CMT1A are generally attributed to length-dependent large-fiber dysfunction (loss of touch, vibration, and position sense in the lower limbs). However, it has become increasingly evident that small-diameter sensory nerves must also be affected, as was previously hypothesized and reported anecdotally.^{49,50} C unmyelinated and A- δ small myelinated nerve

fibers carry pain and temperature modalities that terminate in the skin as ENFs.⁵¹ The reduction in ENF density would therefore explain the length-dependent reduction of pain and temperature sensation observed in most patients with CMT1A.^{52,53} Abnormalities in these nerves may also explain the pain that occurs in some patients with CMT1A. Pain is a common problem in CMT1A that may begin in childhood⁵⁴ and impairs quality of life in both children⁵⁵ and adults^{56,57}. While much of the pain may be related to structural or joint abnormalities that are present from childhood,⁵⁴ neuropathic pain has been estimated to occur in approximately 20% of patients with CMT1A.⁵⁸ A study using LEPs to explore the nociceptive pathway in 16 patients with CMT1A reported a length-dependent impairment of A- δ fibers.⁵⁹ Our study also supports the involvement of A- δ fibers in CMT1A since these are myelinated, and PMP22 has a fundamental role in myelination.⁶⁰ However, some of our findings (warm threshold abnormalities and ENF loss) also suggest an involvement of C fibers in CMT1A, although we cannot have morphologic evidence, since it is not possible to distinguish between C and A- δ fibers, whose cutaneous terminal branches are both unmyelinated.^{36,61} The involvement of small fibers in conditions affecting mainly large fibers has been previously reported,⁶²⁻⁶⁴ implying that congenital or acquired mechanisms underlying the degeneration of large fibers may also affect small fibers. In CMT1A, abnormalities of the interaction between axon and Schwann cells may play a causative role in the distal degeneration of unmyelinated fibers, since PMP22 is also present in the plasma membrane of nonmyelinating Schwann cells.⁶⁵ In addition, although the exact role of PMP22 is still under investigation, it has been observed that PMP22 overexpression may affect Schwann cell proliferation, differentiation, and death.⁶⁶ The correlation of ENF loss with both MC density and tactile thresholds suggests that small fiber and large fiber degeneration in CMT1A follow a parallel course. ENF loss substantially increased with age, suggesting an additive effect on the modest decline in density observed in normal cohorts of controls.⁶⁷ This decline could not be appreciated in our age- and sex-matched control population representing a small cohort with a nonhomogeneous distribution of subjects among the different age decades.

Autonomic nerves

The autonomic nervous system (ANS) is divided into sympathetic and parasympathetic components. Along the sympathetic pathway, only preganglionic sympathetic fibers are myelinated.⁶⁸ Preganglionic sympathetic fibers originate from the spinal cord in the Clarke column and project to peripheral sympathetic ganglia. Preganglionic parasympathetic fibers originate from neurons located in the brainstem or sacral spinal cord and have a long course before the synapsis in the parasympathetic ganglia sited close to their target organs. In general, it is widely thought that signs and symptoms of ANS involvement such as urinary dysfunction, gastrointestinal disturbances, or orthostatic complaints are unusual in CMT1A patients.⁵² For example, prior reports have found that cardiac dysautonomia is relatively uncommon in CMT1A.⁶⁹ Despite the low occurrence of CVR abnormalities, we observed a moderate loss of vasomotor nerves in all our patients. This discrepancy was in some way expected. In fact, we have learned from other longstanding autonomic conditions that cutaneous vasomotor denervation may not be associated with CVR abnormalities.⁷⁰ Alternatively, we found abnormalities of sweating, sympathetically mediated, to be frequent. In our patient population, through the SFN-oriented questionnaire, hypohidrosis emerged as the most frequently reported autonomic symptom (60%). We evaluated the entire polysynaptic sudomotor pathway using SSR and also used DST to explore the function of postganglionic sudomotor nerves. SSR was present in all our patients but the amplitude of the potentials in the distal site was lower compared to healthy age and sex-matched controls. For diagnostic purposes only, the absence of the response is considered abnormal; however, SSR amplitude has been recently shown to correlate with sweat output.⁷¹ DST revealed hypohidrosis in 70% of our patients. DST is an objective and reliable test that is independent of patient cooperation.³⁴ Both SSR and DST indicated a sudomotor functional impairment that goes parallel to the loss of sudomotor nerves. Taken together, our data demonstrate that some autonomic abnormalities are present in patients with CMT1A. Why some modalities are more affected than others and whether abnormalities result from dysfunction of presynaptic sympathetic fibers is beyond the scope of the present manuscript

but will be important in understanding the pathogenesis of clinical abnormalities in patients with CMT1A.

We demonstrated through morphologic, physical, and psychophysical testing that small somatic nerve fibers and some sympathetic autonomic fibers are abnormal and cause symptoms in patients with CMT1A. Our findings build on a small but growing body of research that aims to demonstrate that CMT1A not only affects large myelinated fibers but also involves small fibers. Since SFN-related disturbances can negatively affect the clinical picture and the quality of life of patients with CMT1A, awareness of such symptoms by the clinician could lead to better treatment and an improvement of disease course.

6.2 Large fiber involvement in different CMT subtypes

Morphological data from patients with CMT is essential to understand the consequences of CMT causing mutations in patients and to compare abnormalities in humans with those in animal or cellular models of the same mutations. Sural nerve biopsies are no longer routinely performed in patients with CMT because they are invasive and not necessary for making a genetic diagnosis. We provided additional evidence that morphological data from minimally invasive skin biopsies offer similar information to that provided by sural nerve biopsies by identifying abnormalities in myelin or axons resulting from mutations in CMT causing genes. These morphological abnormalities provide interesting insights into potential pathomechanisms of axonal and demyelinating CMT as described below.

Axonal loss

Axonal degeneration is a major cause of long-term disability in both demyelinating and axonal CMT.⁷² Skin biopsy studies have previously demonstrated a loss of MC, a consequence of axonal loss, in patients with CMT1⁷³ and CMT1A²³. In addition, recent observations using “in vivo confocal microscopy” demonstrated a significant correlation between MC loss and clinical disability as assessed by CMTNS.⁷⁴ We have extended these observations in our studies by observing reductions in the density of both MC and IME in skin samples from multiple patients with axonal (*TRPV4*, *RAB7*, *GDAP1*) and “intermediate” (late onset *MPZ* and *GJB1*) forms of CMT in

addition to patients with CMT1A. We did not find a significant correlation between MC or IME loss and the CMTNS. However, our AR-CMT2K patient who presented with the most severe clinical impairment (CMTNS= 20) had a complete loss of MC and IME at skin biopsy. Taken together, our results demonstrate that axonal loss in CMT can be readily detected by skin biopsy. Since skin biopsies can be performed on multiple occasions these results also suggest their potential use as an outcome measure to detect axonal loss in longitudinal studies.

Nodal gap length

Nodes of Ranvier, paranodes and juxtaparanodes contain specialized regions of myelin and the axonal cytoskeleton that play important roles in developing and maintaining the organization of myelin and the ensheathed axon.⁷⁵ Altered axon-glia communication at this level has been hypothesized to contribute to axonal degeneration in patients with CMT1A and CMTX1.^{22,76} Abnormalities and reorganization of paranodal regions have been clearly documented in sural and dermal nerve fibres from patients with CMT1A and CMTX1.^{22,77,78} Retraction of paranodal myelin appears as a widening of the nodal gap, which includes the true nodal space and part of flanking paranodal regions. Thus widening of nodal gaps can be used as a surrogate marker for changes occurring at nodes and/or paranodes. Evidence of widened gaps was observed in Trembler-J⁷⁹ and Cx32-deficient mice⁸⁰. We found that nodal gaps were significantly larger in patients with CMT1A than in other genotypes suggesting that widening of the nodal gap may be a feature of CMT subtypes that affect myelin. However, we also found that nodal gaps were wider in all other genotypes compared to controls suggesting that nodal gaps are abnormal even in patients with axonal forms of CMT. Abnormalities of nodal gaps have not been previously described in patients with CMT2 but experimental models of axonal degeneration have shown that early structural changes include paranodal myelin retraction.^{81,82} Moreover, retracted paranodal myelin sheaths are frequently associated with swollen axons⁸³ which are thought to represent pre-degenerative phenomena⁸⁴. These abnormalities were widely observed in dermal nerve fibres from our patients. Perhaps altered communications between axons and glia are common features for multiple forms of CMT

including those that primarily affect axons though widening may be greater in the de or dysmyelinating forms such as CMT1A.

Internodal length

Uniformly short internodes occur in dysmyelinating models such as periaxin null mice and have been hypothesized to cause slow nerve conduction velocities such as are seen in these mice and in patients with periaxin mutations causing CMT4F.⁸⁵ Uniformly shortened internodes in dermal nerve fibres were previously observed in skin biopsies from patients with CMT1A suggesting that developmental abnormalities in internode formation contributed to the slow nerve conduction velocities in patients.²³ However, shortened internodes have been reported in a sural nerve biopsy from a single late-onset axonal *MPZ*-mutated patient⁸⁶ and in peripheral nerves of mutant mice deficient for *Cx32*⁸⁰. Patients with late onset CMT1B or with *CMTX1* often have normal or only mildly slowed nerve conduction velocities⁸ and minimal evidence of myelin abnormalities morphologically^{87,88}. In the current paper we observed shortened internodes in all the CMT genotypes. Therefore, while uniformly shortened internodes may suggest a developmental abnormality in internode formation it is unclear whether they are always associated with abnormal myelin and whether they alone always cause slow conduction velocities. We would not find it surprising that developmental abnormalities in axonal neuropathies could result in shortened internodes if we consider that reciprocal interactions between Schwann cells and axons are critical for the development of myelinated axons.^{89,90} Therefore mutations in both myelin and axon genes may developmentally impede internode formation. It will be interesting to investigate internodal length in skin biopsies with severe, early onset dysmyelinating CMT to determine whether it is the extent of the shortening of internodes rather than the presence or absence of shortening that best correlates with abnormalities of myelination.

Effects of nodal and internodal length on nerve conduction velocity

The question remains of why conduction velocities would be normal or near normal in axonal neuropathies if they, like demyelinating neuropathies also have shortened internodes. A potential answer to this question is provided in the recent study demonstrating that nerve conduction velocity in myelinated

nerves relies on internodal length until a threshold of internodal distance is reached, beyond which conduction speed does not increase further.⁹¹ We hypothesize that shortened internodes will therefore not cause slow conduction velocities until the shortening crosses this threshold. Consistent with this hypothesis, our patients with CMT1A had the shortest internodal length of all our patients. Moreover, CMT1A patients also had the widest nodal gap of our patients. The nodal/paranodal region represents an essential region for saltatory conduction in myelinated nerve fibres. Paranodal demyelination and abnormal exposure of voltage gated potassium channels at the paranodal regions can delay the rise time of action potentials, and may further contribute to NCV slowing. It may be that the extent of internodal shortening and nodal gap widening are both important in causing uniformly slow nerve conduction in CMT1A.

6.3 Reduced neurofilament expression in cutaneous nerve fibers of patients with CMT2E

Our results demonstrated a reduced expression of neurofilament and smaller axonal diameter in cutaneous nerve fibers of patients with CMT2E. In addition, our findings did not show NF aggregates in the axons, suggesting that their proximal localization in the cell body may lead to NF disruption distally. The cytoskeletal perturbation is specific for NF and does not affect other components involved in the axonal transport and scaffold, and in nodal/paranodal architecture.

NF are the intermediate filaments of neurons and one of the major components of the neuronal cytoskeleton. They have a tripartite structure made up of a head domain which is involved in the assembly, a central rod domain that plays a role in the formation of filamentous structures, and a tail domain by which NF interacts with other components of the cytoskeleton.⁹² They are modified by post-translational changes and the most significant of these changes is phosphorylation. Their function appears to be intimately related to their phosphorylation state. *NEFL*-linked CMT2E mutations are distributed throughout the three functional domains and different mutations have been shown to cause distinct pathological effect.^{44,93} The mutation carried by our patients that leads to a substitution of glutamic acid to lysine at position 396

(Glu396Lys), occurs in a highly conserved motive at the end of the rod domain and several families with the same mutation as well as a transgenic mouse model have been reported in literature.^{42-44,93-95} The axons of the mutant mouse had fewer NF than those of the wild-type, and accordingly sural nerve biopsies from patients have shown the presence of axons either devoid or with a variable density of NF. Our results from both IHC and WB analysis are in keeping with these data, demonstrating reduced levels of NF in cutaneous nerve fibers. We think that a decrease in NF abundance in peripheral nerves might be a pathological marker of CMT2E and independent from the axonal loss. Specifically, the Glu396Lys mutation, as occurs in a protein domain involved in the dimerization process, may affect the ability of NF to assembly properly into filaments, disrupting the NF network and reducing the transport of NF into the axons. The loss of axonal NF distally may be a consequence of their accumulation proximally in both nerve fiber and cell body (as shown in transgenic models and iPSC-derived motor neurons from a CMT2E patient⁹⁶), leading to the formation of aggregates and to subsequent alterations in the axonal cytoskeleton. The lack of NF aggregates distally supports this hypothesis. Notably, Fabrizi et al.⁴³ reported the presence of giant axons with NF accumulation in sural nerve biopsies from four CMT2E patients carrying three different *NEFL* mutations, but not in their patient with the Glu396Lys mutation. This findings confirm that different mutations behave differently as far as disruption of NF organization is concerned, and that abnormalities of NF organization may be a marker of CMT2E. The possible alteration of axonal transport due to NF disruption does not involve other molecules that play a role in this process. Indeed, we did not find either an increase or a defect in the expression of acetylated α -tubulin as respectively shown in *NEFL* knockout mice and in other models of axonal CMT.^{97,98}

A linear relationship between conduction velocity and fiber diameter is well known.⁹⁹ Reduction in axon diameter decreases velocity, largely because the longitudinal resistance is higher. The most essential function of NF is regulating the axonal caliber and thereby the conduction velocity. NF are therefore particularly abundant in neurons with large diameter axons where fast impulse conduction velocities are crucial for proper functioning.¹⁰⁰ Within the skin, NF is expressed by both A δ - and A β -fibers, which are fast conducting

nerve fibres, but not by C-fibers that conduct more slowly.¹⁰¹ In transgenic mice the loss of NF-L resulted in axons with reduced diameters and slowed conduction velocities.^{97,102} Morphometric analysis of sural nerve biopsies from CMT2E patients disclosed decreased axonal diameters in myelinated fibers.^{42,43} Our morphometric data demonstrated that reduced axonal diameters can also be detected in a less invasive way in cutaneous nerve fibers. These smaller axonal calibers can explain the slow conduction velocities observed in CMT2E, supporting the notion that conduction velocity can be slow even in the absence of demyelination or abnormalities of nodes and paranodes, since no significant myelin sheath, nodal or paranodal abnormalities were detected in our patients. Although the decreased axonal caliber observed in our patient might be the consequence of the loss of large diameter fibers. Indeed, mice in which NF-L has been deleted (NF-L -/-) showed a unimodal distribution of axon calibers with the large-sized myelinated axons being shifted to the small size axons, and a reduction in the large diameter fibres with loss of the bimodal spectrum have been reported in CMT2E patients as well.^{44,93,97} We believe that both phenomena occur in CMT2E and, along with the normal molecular architecture of nodes and paranodes, explain the reduced velocities detected in CMT2E patients.

In conclusion, our study extends the pathology of CMT2E and provides clues to the pathogenesis, supporting the feasibility of skin biopsy to investigate its mechanisms. A better understanding of the pathomechanism underlying each single *NEFL* mutation can lead to identify a clear genotype-phenotype correlation.

7. CONCLUSIONS

Morphological data from patients with CMT is essential to understand the consequences of CMT causing mutations in patients and to compare abnormalities in humans with those in animal or cellular models of the same mutations. Sural nerve biopsies are no longer routinely performed in patients with CMT because they are invasive and not necessary for making a genetic diagnosis. We provided additional evidence that morphological data from minimally invasive skin biopsies offer similar information to that provided by sural nerve biopsies by identifying abnormalities in myelin or axons resulting

from mutations in CMT causing genes. The morphological abnormalities discussed above provide interesting insights into potential pathomechanisms of axonal and demyelinating CMT.

In details, this study extends the information gained from skin biopsies on morphological abnormalities in various forms of CMT. We have shown the impairment of unmyelinated fibers in a demyelinated form of CMT. We have demonstrated that myelinated dermal nerves can be used to detect axonal degeneration and changes in nodal and paranodal regions as well as in internodal length in both axonal and demyelinating forms of CMT. It will be important to extend these investigations into patients with severe dysmyelinating forms of CMT such as early onset CMT1B or CMT4 to determine whether widening of nodal gaps or shortening of internodes is even more pronounced in these disorders. Moreover, our study extends the pathology of CMT2E and provides clues to the pathogenesis, supporting the feasibility of skin biopsy to investigate its mechanisms. A better understanding of the pathomechanism underlying each single *NEFL* mutation can lead to identify a clear genotype-phenotype correlation.

Lastly, since this minimally invasive procedure can easily be repeated in the same subject, it could provide a morphological marker of disease progression in both natural history and clinical trials.

8. REFERENCES

1. Pisciotta C, Shy ME. Genetic neuropathy. *Handb Clin Neurol* (in press 2015).
2. Kazamel M, Boes CJ. Charcot Marie Tooth disease (CMT): historical perspectives and evolution. *J Neurol* 2014.
3. Pisciotta C, Shy ME. The Inherited Peripheral Neuropathies. In: *Merritt's Neurology* 13th edition. Lippincott Williams & Wilkins; 2014.
4. Rossor AM, Polke JM, Houlden H, et al. Clinical implications of genetic advances in Charcot-Marie-Tooth disease. *Nat Rev Neurol* 2013.
5. Landrieu P, Baets J. Early onset (childhood) monogenic neuropathies. *Handb Clin Neurol* 2013.

6. Murphy SM, Laura M, Fawcett K, et al. Charcot-Marie-Tooth disease: frequency of genetic subtypes and guidelines for genetic testing. *J Neurol Neurosurg Psychiatry* 2012.
7. Gess B, Schirmacher A, Boentert M, et al. Charcot-Marie-Tooth disease: frequency of genetic subtypes in a German neuromuscular center population. *Neuromuscul Disord* 2013.
8. Saporta AS, Sottile SL, Miller LJ, et al. Charcot-Marie-Tooth disease subtypes and genetic testing strategies. *Ann Neurol* 2011.
9. Sivera R, Sevilla T, Vílchez JJ, et al. Charcot-Marie-Tooth disease: genetic and clinical spectrum in a Spanish clinical series. *Neurology* 2013.
10. Manganelli F, Tozza S, Pisciotta C, et al. Charcot-Marie-Tooth disease: frequency of genetic subtypes in a Southern Italy population. *J Peripher Nerv Syst* 2014.
11. Saporta MA, Shy ME. Inherited peripheral neuropathies. *Neurol Clin* 2013.
12. Pareyson D, Marchesi C, Salsano E. Dominant Charcot-Marie-Tooth syndrome and cognate disorders. *Handb Clin Neurol* 2013.
13. Klein CJ, Duan X, Shy ME. Inherited neuropathies: clinical overview and update. *Muscle Nerve* 2013.
14. Harel T, Lupski JR. Charcot-Marie-Tooth disease and pathways to molecular based therapies. *Clin Genet* 2014.
15. Colby J, Nicholson R, Dickson KM, et al. PMP22 carrying the trembler or trembler-J mutation is intracellularly retained in myelinating Schwann cells. *Neurobiol Dis* 2000.
16. Pennuto M, Tinelli E, Malaguti M, et al. Ablation of the UPR-mediator CHOP restores motor function and reduces demyelination in Charcot-Marie-Tooth 1B mice. *Neuron* 2008.
17. Saporta MA, Shy BR, Patzko A, et al. MpzR98C arrests Schwann cell development in a mouse model of early-onset Charcot-Marie-Tooth disease type 1B. *Brain* 2012.
18. Khajavi M, Shiga K, Wiszniewski W, et al. Oral curcumin mitigates the clinical and neuropathologic phenotype of the Trembler-J mouse: a potential therapy for inherited neuropathy. *Am J Hum Genet* 2007.

19. Patzko A, Bai Y, Saporta MA, et al. Curcumin derivatives promote Schwann cell differentiation and improve neuropathy in R98C CMT1B mice. *Brain* 2012.
20. Gentil BJ, Cooper L. Molecular basis of axonal dysfunction and traffic impairments in CMT. *Brain Res Bull* 2012.
21. Lauria G, Hsieh ST, Johansson O et al.; European Federation of Neurological Societies; Peripheral Nerve Society. European Federation of Neurological Societies/Peripheral Nerve Society Guideline on the use of skin biopsy in the diagnosis of small fiber neuropathy. Report of a joint task force of the European Federation of Neurological Societies and the Peripheral Nerve Society. *Eur J Neurol* 2010.
22. Li J, Bai Y, Ghandour K, et al. Skin biopsies in myelin-related neuropathies: bringing molecular pathology to the bedside. *Brain* 2005.
23. Saporta MA, Katona I, Lewis RA, et al. Shortened internodal length of dermal myelinated nerve fibres in Charcot-Marie-Tooth disease type 1A. *Brain* 2009.
24. Katona I, Wu X, Feely SM, et al. PMP22 expression in dermal nerve myelin from patients with CMT1A. *Brain* 2009.
25. Nobbio L, Visigalli D, Radice D, et al. PMP22 messenger RNA levels in skin biopsies: testing the effectiveness of a Charcot-Marie-Tooth 1A biomarker. *Brain* 2014.
26. Krajewski KM, Lewis RA, Fuerst DR, et al. Neurological dysfunction and axonal degeneration in Charcot-Marie-Tooth disease type 1A. *Brain* 2000.
27. Nolano M, Manganelli F, Provitera V, et al. Small nerve fiber involvement in CMT1A. *Neurology* 2015.
28. Manganelli F, Nolano M, Pisciotta C, et al. Charcot–Marie-Tooth disease: new insights from skin biopsy. *Neurology* 2015.
29. Pisciotta C, Bai Y, Brennan KM, et al. Reduced neurofilament expression in cutaneous nerve fibers of patients with CMT2E. *Neurology* 2015.

30. Shy ME, Blake J, Krajewski K, et al. Reliability and validity of the CMT neuropathy score as a measure of disability. *Neurology* 2005.
31. Murphy SM, Herrmann DN, McDermott MP, et al. Reliability of the CMT neuropathy score (second version) in Charcot-Marie-Tooth disease. *J Peripher Nerv Syst* 2011.
32. Nolano M, Provitera V, Crisci C, et al. Quantification of myelinated endings and mechanoreceptors in human digital skin. *Ann Neurol* 2003.
33. Donadio V, Nolano M, Provitera V, et al. Skin sympathetic adrenergic innervation: an immunofluorescence confocal study. *Ann Neurol* 2006.
34. Nolano M, Provitera V, Caporaso G, et al. Quantification of pilomotor nerves: a new tool to evaluate autonomic involvement in diabetes. *Neurology* 2010.
35. Provitera V, Nolano M, Caporaso G, et al. Postganglionic sudomotor denervation in patients with multiple system atrophy. *Neurology* 2014.
36. Provitera V, Nolano M, Pagano A, et al. Myelinated nerve endings in human skin. *Muscle Nerve* 2007.
37. Taylor LE, Kaminoh YJ, Rodesch CK, et al. Quantification of dystrophin immunofluorescence in dystrophinopathy muscle specimens. *Neuropathol Appl Neurobiol* 2012.
38. Bakkers M, Faber CG, Hoeijmakers JG, et al. Small fibers, large impact: quality of life in small-fiber neuropathy. *Muscle Nerve* 2014.
39. Nolano M, Provitera V, Estraneo A, et al. Sensory deficit in Parkinson's disease: evidence of a cutaneous denervation. *Brain* 2008.
40. Provitera V, Nolano M, Caporaso G, et al. Evaluation of sudomotor function in diabetes using the dynamic sweat test. *Neurology* 2010.
41. Vita G, Princi P, Calabro R, et al. Cardiovascular reflex tests: assessment of age adjusted normal range. *J Neurol Sci* 1986.
42. Züchner S, Vorgerd M, Sindern E, et al. The novel neurofilament light (NEFL) mutation Glu397Lys is associated with a clinically and morphologically heterogeneous type of Charcot-Marie-Tooth neuropathy. *Neuromuscul Disord* 2004.

43. Fabrizi GM, Cavallaro T, Angiari C, et al. Charcot-Marie-Tooth disease type 2E, a disorder of the cytoskeleton. *Brain* 2007.
44. Shen H, Barry DM, Dale JM, et al. Muscle pathology without severe nerve pathology in a new mouse model of Charcot-Marie-Tooth disease type 2E. *Hum Mol Genet* 2011.
45. Tradewell ML, Durham HD, Mushynski WE, et al. Mitochondrial and axonal abnormalities precede disruption of the neurofilament network in a model of Charcot-Marie-Tooth disease type 2E and are prevented by heat shock proteins in a mutant-specific fashion. *J Neuropathol Exp Neurol* 2009.
46. Griffin JW, Watson DF. Axonal transport in neurological disease. *Ann Neurol* 1988.
47. Hoffman PN, Griffin JW, Price DL. Control of axonal caliber by neurofilament transport. *J Cell Biol* 1984.
48. Perrot R, Lonchamp P, Peterson AC, et al. Axonal neurofilaments control multiple fiber properties but do not influence structure or spacing of nodes of Ranvier. *J Neurosci* 2007.
49. Shy M, Lupski JR, Chance PF, et al. The hereditary motor and sensory neuropathies: an overview of the clinical, genetic, electrophysiologic and pathologic features. In: Dyck PJ, Thomas PK, eds. *Peripheral Neuropathy*, 4th ed. Philadelphia: WB Saunders; 2005.
50. Brooks AP. Abnormal vascular reflexes in Charcot-Marie-Tooth disease. *J Neurol Neurosurg Psychiatry* 1980.
51. Shy ME. Peripheral neuropathies. In: Shafer G, ed. *Goldman's Cecil Medicine*. Philadelphia: 2012.
52. Thomas PK, Marques W, Davis MB, et al. The phenotypic manifestations of chromosome 17p11.2 duplication. *Brain* 1997.
53. Krajewski KM, Lewis RA, Fuerst DR, et al. Neurological dysfunction and axonal degeneration in Charcot-Marie-Tooth disease type 1A. *Brain* 2000.
54. Ramchandren S, Jaiswal M, Feldman E, et al. Effect of pain in pediatric inherited neuropathies. *Neurology* 2014.

55. Burns J, Ramchandren S, Ryan MM, et al. Determinants of reduced health-related quality of life in pediatric inherited neuropathies. *Neurology* 2010.
56. Colomban C, Micallef J, Lefebvre MN, et al. Clinical spectrum and gender differences in a large cohort of Charcot-Marie-Tooth type 1A patients. *J Neurol Sci* 2014.
57. Padua L, Shy ME, Aprile I, et al. Correlation between clinical/neurophysiological findings and quality of life in Charcot-Marie-Tooth type 1A. *J Peripher Nerv Syst* 2008.
58. Laura M, Hutton EJ, Blake J, et al. Pain and small fiber function in Charcot-Marie-Tooth disease type 1A. *Muscle Nerve* 2014.
59. Pazzaglia C, Vollono C, Ferraro D, et al. Mechanisms of neuropathic pain in patients with Charcot-Marie-Tooth 1A: a laser-evoked potential study. *Pain* 2010.
60. Trapp BD, Pfeiffer SE, Anitei A, et al. Cell biology and myelin assembly. In: Lazzarini RA, ed. *Myelin Biology and Disorders*. San Diego: Elsevier Academic Press; 2003.
61. Voyvodic JT. Target size regulates calibre and myelination of sympathetic axons. *Nature* 1989.
62. Nolano M, Provitera V, Crisci C, et al. Small fibers involvement in Friedreich's ataxia. *Ann Neurol* 2001.
63. Pan CL, Tseng TJ, Lin YH, et al. Cutaneous innervation in Guillain-Barré syndrome: pathology and clinical correlations. *Brain* 2003.
64. Ruts L, van Doorn PA, Lombardi R, et al. Unmyelinated and myelinated skin nerve damage in Guillain-Barré syndrome: correlation with pain and recovery. *Pain* 2012.
65. Haney C, Snipes GJ, Shooter EM, et al. Ultrastructural distribution of PMP22 in Charcot-Marie-Tooth disease type 1A. *J Neuropathol Exp Neurol* 1996.
66. Li J, Parker B, Martyn C, et al. The PMP22 gene and its related diseases. *Mol Neurobiol* 2013.
67. Lauria G, Bakkers M, Schmitz C, et al. Intraepidermal nerve fiber density at the distal leg: a worldwide normative reference study. *J Peripher Nerv Syst* 2010.

68. Gardner ED, Bunge RP. Gross anatomy of the peripheral nervous system. In: Dyck PJ, Thomas PK, eds. *Peripheral Neuropathy*, 4th ed. Philadelphia: Elsevier; 2005.
69. Ingall TJ, McLeod JG. Autonomic function in hereditary motor and sensory neuropathy (Charcot-Marie-Tooth disease). *Muscle Nerve* 1991.
70. Nolano M, Provitera V, Perretti A, et al. Ross syndrome: a rare or a misknown disorder of thermoregulation? A skin innervation study on 12 subjects. *Brain* 2006.
71. Ellaway PH, Kuppuswamy A, Nicotra A, et al. Sweat production and the sympathetic skin response: improving the clinical assessment of autonomic function. *Auton Neurosci* 2010.
72. Suter U, Scherer SS. Disease mechanisms in inherited neuropathies. *Nat Rev Neurosci* 2003.
73. Dyck PJ, Winkelmann RK, Bolton CF. Quantitation of Meissner's corpuscles in hereditary neurologic disorders. Charcot-Marie-Tooth disease, Roussy-Levy syndrome, Dejerine-Sottas disease, hereditary sensory neuropathy, spinocerebellar degenerations, and hereditary spastic paraplegia. *Neurology* 1966.
74. Almodovar JL, Ferguson M, McDermott MP, et al. In vivo confocal microscopy of Meissner corpuscles as a novel sensory measure in CMT1A. *J Peripher Nerv Syst* 2011.
75. Scherer SS, Arroyo EJ. Recent progress on the molecular organization of myelinated axons. *J Peripher Nerv Syst* 2002.
76. Sousa AD, Bhat MA. Cytoskeletal transition at the paranodes: the Achilles' heel of myelinated axons. *Neuron Glia Biol* 2007.
77. Hahn AF, Ainsworth PJ, Bolton CF, et al. Pathological findings in the X-linked form of Charcot-Marie-Tooth disease: a morphometric and ultrastructural analysis. *Acta Neuropathol* 2001.
78. Hattori N, Yamamoto M, Yoshihara T, et al. Demyelinating and axonal features of Charcot-Marie-Tooth disease with mutations of myelin-related proteins (PMP22, MPZ and Cx32): a clinicopathological study of 205 Japanese patients. *Brain* 2003.

79. Devaux JJ, Scherer SS. Altered ion channels in an animal model of Charcot-Marie-Tooth disease type IA. *J Neurosci* 2005.
80. Neuberg DH, Sancho S, Suter U. Altered molecular architecture of peripheral nerves in mice lacking the peripheral myelin protein 22 or connexin32. *J Neurosci Res* 1999.
81. Spencer PS, Schaumburg HH. Ultrastructural studies of the dying-back process. III. The evolution of experimental peripheral giant axonal degeneration. *J Neuropathol Exp Neurol* 1977.
82. Veronesi B, Peterson ER, Bornstein MB, et al. Ultrastructural studies of the dying-back process. VI. Examination of nerve fibers undergoing giant axonal degeneration in organotypic culture. *J Neuropathol Exp Neurol* 1983.
83. Griffin JW, Drucker N, Gold BG, et al. Schwann cell proliferation and migration during paranodal demyelination. *J Neurosci* 1987.
84. Ebenezer GJ, McArthur JC, Thomas D, et al. Denervation of skin in neuropathies: the sequence of axonal and Schwann cell changes in skin biopsies. *Brain* 2007.
85. Court FA, Sherman DL, Pratt T, et al. Restricted growth of Schwann cells lacking Cajal bands slows conduction in myelinated nerves. *Nature* 2004.
86. Laurà M, Milani M, Morbin M, et al. Rapid progression of late onset axonal Charcot-Marie-Tooth disease associated with a novel MPZ mutation in the extracellular domain. *J Neurol Neurosurg Psychiatry* 2007.
87. Li J, Bai Y, Ianakova E, et al. Major myelin protein gene (P0) mutation causes a novel form of axonal degeneration. *J Comp Neurol* 2006.
88. Kleopa KA, Abrams CK, Scherer SS. How do mutations in GJB1 cause X-linked Charcot-Marie-Tooth disease? *Brain research* 2012.
89. Woodhoo A, Sommer L. Development of the Schwann cell lineage: from the neural crest to the myelinated nerve. *Glia* 2008.
90. Taveggia C, Feltri ML, Wrabetz L. Signals to promote myelin formation and repair. *Nat Rev Neurol* 2010.

91. Wu LM, Williams A, Delaney A, et al. Increasing internodal distance in myelinated nerves accelerates nerve conduction to a flat maximum. *Curr Biol* 2012.
92. Holmgren A, Bouhy D, Timmerman V. Neurofilament phosphorylation and their proline-directed kinases in health and disease. *J Peripher Nerv Syst* 2012.
93. Perez-Olle R, Jones ST, Liem RK. Phenotypic analysis of neurofilament light gene mutations linked to Charcot-Marie-Tooth disease in cell culture models. *Hum Mol Genet* 2004.
94. Elbracht M, Senderek J, Schara U, et al. Clinical and morphological variability of the E396K mutation in the neurofilament light chain gene in patients with Charcot-Marie-Tooth disease type 2E. *Clin Neuropathol* 2014.
95. Abe A, Numakura C, Saito K, et al. Neurofilament light chain polypeptide gene mutations in Charcot-Marie-Tooth disease: nonsense mutation probably causes a recessive phenotype. *J Hum Genet* 2009.
96. Saporta MA, Dang V, Volfson D, et al. Axonal Charcot-Marie-Tooth disease patient-derived motor neurons demonstrate disease-specific phenotypes including abnormal electrophysiological properties. *Exp Neurol* 2015.
97. Zhu Q, Couillard-Després S, Julien JP. Delayed maturation of regenerating myelinated axons in mice lacking neurofilaments. *Exp Neurol* 1997.
98. d'Ydewalle C, Krishnan J, Chiheb DM, et al. HDAC6 inhibitors reverse axonal loss in a mouse model of mutant HSPB1-induced Charcot-Marie-Tooth disease. *Nat Med* 2011.
99. Hursh, JB. Conduction velocity and diameter of nerve fibres. *Am J Physiol* 1939.
100. Al-Chalabi A, Miller CC. Neurofilaments and neurological disease. *Bioessays* 2003.
101. Reinisch CM, Tschachler E. The dimensions and characteristics of the subepidermal nerve plexus in human skin-terminal Schwann cells

constitute a substantial cell population within the superficial dermis. *J Dermatol Sci* 2012.

102. Sakaguchi T, Okada M, Kitamura T, et al. Reduced diameter and conduction velocity of myelinated fibers in the sciatic nerve of a neurofilament-deficient mutant quail. *Neurosci Lett* 1993.

Table 1. Specific CMT types.

Type	Gene/locus	Specific phenotype
Autosomal dominant CMT1 (ADCMT1)		
CMT1A	Dup 17p (PMP22)	CMT1
CMT1B	MPZ	CMT1/DSN/intermediate/CMT2
CMT1C	SIMPLE	CMT1
CMT1D	EGR2	CMT1/DSN
CMT1E	PMP22 point mutations	CMT1/DSN
CMT1F	NEFL	CMT2 but can have slow MNCVs with early onset and severe phenotype
Hereditary neuropathy with liability to pressure palsies		
HNPP	Del 17p/PMP22 point mutations	Typical HNPP
X-linked CMT1		
CMTX1	GJB1	Intermediate (male MNCVs < female MNCVs)
Autosomal dominant CMT2 (ADCMT2)		
CMT2A	MFN2	CMT2, usually severe, optic atrophy
CMT2B	RAB7	CMT2 with predominant sensory involvement
CMT2C	TRPV4	CMT2 with vocal cord and respiratory involvement
CMT2D	GARS	CMT2 with predominant hand wasting/weakness or dHMN-V
CMT2E	NEFL	CMT2 but can have slow MNCVs with early onset and severe phenotype
CMT2F	HSP27 (HSPB1)	Classic CMT2 or dHMN-IIB
CMT2L	HSP22 (HSPB8)	Classic CMT2 or dHMN-IIA
CMT2K	GDAP1	Classic CMT2
Autosomal recessive demyelinating CMT (CMT4)		
CMT4A	GDAP1	CMT1, early onset and severe phenotype/vocal cord and diaphragm paralysis
CMT4B1	MTMR2	Severe CMT1/facial/bulbar/focally folded myelin
CMT4C	SH3TC2	CMT1, can be sever/scoliosis
CMT4F	PRX	CMT1/more sensory/focally folded myelin
CMT4J	FIG4	CMT1
Autosomal recessive axonal CMT (AR-CMT2)		
AR-CMT2A	LMNA	CMT2 proximal involvement and rapid progression/cardiomyopathy

AD, autosomal dominant; AR, autosomal recessive; CMT, Charcot–Marie–Tooth; Del, deletion; dHMN, distal hereditary motor neuropathy; DSN, Dejerine Sottas neuropathy; Dup, duplication; EGR2, early growth response 2; FIG4, FIG4 homologue; GARS, glycyl tRNA synthetase; GDAP1, ganglioside induced differentiation associated protein 1; GJB1, gap junction protein beta1; HNPP, hereditary neuropathy with liability to pressure palsies; HSP22, heat shock 22 kDa protein 8; HSP27, heat shock 27 kDa protein 1; LMNA, lamin A/C; MNCV, motor nerve conduction velocity; MFN2, mitofusin 2; MPZ, myelin protein zero; MTMR2, myotubularin related protein 2; NEFL, neurofilament light chain; PMP22, peripheral myelin protein 22; PRX, periaxin; RAB7, RAB7, member RAS oncogene family; SH3TC2, SH3 domain and tetratricopeptide repeats 2; SIMPLE, small integral membrane protein of the lysosome/late endosome.

Table 2. Classic CMT phenotype.

Onset	II decade of life
Onset symptom/sign	Tripping and falling/balance problems
Gait	Steppage gait
Cranial nerves	Usually normal
Weakness	Symmetric, distal > proximal, LL > UL, anterior > posterior leg compartment
Atrophy	Hand and foot intrinsic muscles, leg muscles (inverted champagne bottle legs)
Sensation	Sensory loss in stocking/glove distribution
Balance	Impaired due to proprioception sense loss
Deformities	Claw hand, pes cavus/flat foot, hammer toes, scoliosis
Deep tendon reflexes	Diffusely absent but always involving the Achilles tendon

Table 3. Name, source and dilution of primary antibodies.

Antigen (Abbreviation)	Manufacturer	Dilution
Rabbit protein gene product 9.5 (rPGP)	Biogenesis	1:400
Mouse protein gene product 9.5 (mPGP)	AbD Serotec	1:800
Rabbit vasoactive intestinal peptide (rVIP)	Immunostar	1:1000
Mouse vasoactive intestinal peptide (mVIP)	Santa Cruz Biotechnology	1:300
Mouse collagen IV (mCOLIV)	Chemicon	1:800
Mouse myelin basic protein (mMBP)	Santa Cruz Biotechnology	1:800
Rabbit dopamine beta hydroxylase (rDBH)	Chemicon	1:1000
Rabbit substance P (rSubP)	Immunostar	1:1000
Rabbit calcitonon gene related peptide (rCGRP)	Immunostar	1:1000
Neurofilament-light chain (NF-L)	Thermo Scientific	1:200 (IHC) 1:10000 (WB)
Phosphorylated neurofilament (Phospho NF)	Covance	1:200
Alpha-tubulin (α -tub)	Cell Signaling	1:800 (IHC) 1:1000 (WB)

Table 4. Demographic data and CMTNS of 20 CMT1A patients.

subject	Sex	age	sensory symptoms	motor symptoms legs	motor symptoms arms	pinprick	vibration	strength legs	strength arms	CMAP	SNAP	CMTES	CMTNS
P01	F	42	2	1	1	2	1	1	1	2	4	9	15
P02	F	44	0	1	0	1	1	1	0	1	3	4	8
P03	F	47	1	1	1	2	1	1	1	1	3	8	12
P04	M	29	2	1	0	2	2	2	1	3	4	10	17
P05	F	29	0	1	0	1	2	1	1	2	4	6	12
P06	F	60	1	2	1	2	3	2	2	3	4	13	20
P07	F	36	0	1	0	1	0	0	0	1	4	2	7
P08	M	48	0	0	0	0	0	1	1	1	4	2	7
P09	M	64	0	1	1	0	2	1	1	2	4	6	12
P10	F	43	1	0	0	0	0	1	1	0	4	3	7
P11	F	46	1	0	1	0	1	1	1	1	4	5	10
P12	F	39	1	0	0	0	1	1	1	2	4	4	10
P13	F	40	1	1	1	1	2	0	1	0	3	7	10
P14	F	45	0	1	1	0	2	0	1	1	4	5	10
P15	F	39	0	2	2	0	1	1	1	1	4	7	12
P16	F	40	0	0	0	1	1	1	0	0	1	3	4
P17	F	43	0	0	0	1	1	1	0	1	3	3	7
P18	F	46	2	1	1	1	1	1	1	1	3	8	12
P19	M	35	0	1	0	2	1	1	1	1	4	6	11
P20	M	42	1	0	1	0	1	1	1	1	4	5	10

CMAP= compound motor action potential amplitude; SAP= sensory action potential amplitude; CMTES=Charcot–Marie–Tooth examination score; CMTNS=Charcot–Marie–Tooth neuropathy score.

Table 5. Morphological data of CMT1A patients.

	Sex, M/F	Age, y	FT ENF/mm	MC/mm ²	IME/mm ²	THIGH ENF/mm	LEG ENF/mm
Patients	5/15	42.9 (8.4)	3.3 (2.1)	9.4 (4.7)	28.0 (13.5)	22.4 (4.3)	8.5 (4.8)
Controls	10/30	42.9 (8.4)	7.9 (2.4)	29.8 (9.3)	55.3 (20.3)	25.1 (5.4)	18.0 (5.2)
<i>p</i>			<0.01	<0.01	<0.01	>0.05	<0.01

FT ENF = Epidermal nerve fibers in fingertip; THIGH ENF= Epidermal nerve fibers in thigh; LEG ENF= Epidermal nerve fibers in leg; MC= Meissner corpuscle; IME= Intrapapillary myelinated fiber. Values are mean (SD).

Table 6. Demographic, SFN-SIQ, QST, and autonomic morphological and functional data of CMT1A patients.

	Gender	Age, y	SFN-SIQ score	HAND						FOOT						LEG					SSR amplitude	CVR
				CS	WS	CP	HP	Pin Prick	TTH	CS	WS	CP	HP	Pin Prick	TTH	PGP-ir SNF density	VIP-ir SNF density	Sweat drop density	Sweat output /gland	Sweat output /cm ²		
P1	F	42	18	1,8	3,3	21,7	12,2	50	10,8	7	9,4	28,4	12,4	10	53,9	1,2	0,8	36	2,2	79,3	1,4	0
P2	F	44	18	2,9	3,2	8,2	10,8	40	18,6	3,1	6,3	10,2	15	20	53,9	1,4	1	28	1,9	53,5	1,7	0
P3	F	47	24	0,9	1,1	23,4	12,4	0	83,3	3,2	11,2	28,2	18	0	83,3	0,9	0,8	15	0,7	10,6	0,9	2
P4	M	29	10	1,6	1,9	9,8	8,3	80	10,8	2,5	3,6	10,8	8,4	80	18,6	1,7	1,2	70	3,8	265,2	1,8	0
P5	F	29	6	1,4	1,8	10,5	9,7	80	1,5	2,1	3,1	10,1	9,8	80	2,5	1,7	1,3	69	1,4	95,6	2,1	0
P6	F	60	8	4,1	5,9	30,7	14,2	0	83,3	6	10	32	18	0	83,3	1,3	0,5	49	0,8	40,8	1,9	1
P7	F	36	4	0,7	1,3	12,4	5	40	1,5	5,2	5,1	8,7	10,5	30	10,8	1,3	0,5	49	3,8	187,2	0,3	0
P8	M	48	4	2,6	9,6	26	16,5	50	32,4	9,1	11,2	27,2	15,7	10	53,9	1,2	0,6	32	1,6	52,8	1,2	0
P9	M	64	6	1,5	12,3	8,5	17,3	20	32,4	3,2	6,4	8,2	13,3	30	32,4	1	0,8	4	4,6	18,3	3	0
P10	F	43	12	1,1	1,9	23,9	10,9	60	18,6	8,4	11,6	26,9	16,1	0	83,3	1,6	0,9	66	6,6	437,2	1,3	1
Patients	3/7	44.2 (11.5)	11.0 (6.9)	1.9 (1.0)	4.2 (3.9)	17.5 (8.4)	11.7 (3.7)	42.0 (28.6)	29.3 (30.4)	5.0 (2.5)	7.8 (3.3)	19.1 (10.1)	13.7 (3.4)	26.0 (30.6)	38.7 (31.4)	1.3 (0.3)	0.8 (0.3)	41.8 (22.8)	2.7 (1.9)	124.1 (135.7)	1.6 (0.7)	0.5 (0.7)
Controls	6/14	44.2 (11.5)	n.a.	1.4 (0.6)	1.7 (0.5)	9.9 (4.3)	7.5 (2.2)	85.2 (15.6)	2.2 (1.1)	3.1 (1.3)	7.6 (2.8)	8.9 (3.0)	8.9 (3.0)	78.4 (17.5)	3.4 (3.5)	2.1 (0.4)	1.7 (0.4)	75.4 (17.5)	9.0 (3.2)	681.2 (332.9)	5.4 (4.8)	n.a.
<i>p</i>				>0.05	>0.05	<0.05	<0.01	<0.01	<0.01	<0.01	<0.01	<0.01	<0.01	<0.01	<0.01	<0.01	<0.01	<0.01	<0.01	<0.01	<0.01	n.a.

Abbreviations: CP= cold pain; CS= cold sensation; CVR= cardiovascular reflexes; HP= heat pain; ir= immunoreactive; NA= not applicable; PGP= protein gene product; QST= quantitative sensory testing; SFNSIQ= Small Fiber Neuropathy Symptoms Inventory Questionnaire; SNF= sudomotor nerve fiber; SSR= sympathetic skin response; TTH= tactile threshold; VIP= vasoactive intestinal peptide; WS= warm sensation.

Thermal thresholds are expressed as °C (Δ from 32° baseline); pinprick is expressed as % of stimuli perceived as painful; TTH is expressed as mN; PGP-ir and VIP-ir SNF density are expressed as nm/ μ m³; sweat gland density is expressed as number of glands/cm²; sweat output is expressed as nL/min; SSR amplitude is registered from feet after electrical stimulation of median nerve and is expressed as mV. The number of CVR tests that gave pathologic results is reported. SD are presented in parentheses.

Table 7. Clinical and skin biopsy features of the CMT group for the large fiber evaluation.

	<i>PMP22</i>	<i>MPZ</i>	<i>GJB1</i>	<i>RAB7</i>	<i>TRPV4</i>	<i>GDAP1</i>	Controls	p value
Individuals (n)	10	5	9	3	3	1	45	
Age (years)	40.4 ± 5.4	52.8 ± 12.3	48.4 ± 13.6	45.6 ± 2.5	42.0 ± 16.0	31	46.5 ± 10.6	NS ^b
Gender (M:F)	2:8	3:2	2:7	2:1	2:1	0:1	21:24	
MNCV (m/sec)^a	21 ± 6.1 (6.2-27.6)	38.9 ± 4.0 (33.1-42)	42.2 ± 7.3 (29.7-48.4)	48.5 ± 6.1 (41.5-52.4)	47.6 ± 4.1 (43-51)	39.3 (31-43)	NA	
CMTNS^a	11.5 ± 2.7 (8-17)	12 ± 1.9 (10-15)	10.4 ± 6.2 (2-17)	10 ± 5.2 (4-14)	17.6 ± 4.0 (14-22)	20	NA	NS ^c
MC (per mm²)^a	8.2 ± 4.7 (2.7-19.6)	4.6 ± 5.5 (0-13.5)	8.2 ± 6.9 (0-23.5)	3.1 ± 3.8 (0-7.6)	0.2 ± 0.4 (0-0.8)	0	28.3 ± 9.2 (14.6-51.9)	< 0.005 ^c
IME (per mm²)^a	28.2 ± 18.7 (1.5-59.8)	20.0 ± 16.1 (0-37.7)	28.0 ± 14.7 (0-52.5)	11.9 ± 4.8 (6.5-15.7)	19.7 ± 19 (3.4-41.9)	0	55.4 ± 21.1 (26.3-100)	< 0.005 ^c
Nodal gap length (µm)^a	n= 263 6.0 ± 3.5 (1.5-22.8)	n= 92 5.1 ± 2.7 (1.7-18.4)	n= 308 4.9 ± 2.0 (1.7-18.6)	n= 62 4.7 ± 2.0 (2.1-13.6)	n= 101 4.4 ± 1.5 (2.1-9.1)	n= 48 4.3 ± 1.4 (2.2-11.9)	n= 234 3.4 ± 1.5 (1.5-11.6)	< 0.0001 ^c
Internodal length (µm)^a	n= 90 53.5 ± 22.4 (20.9-117.2)	n= 23 68.9 ± 36.6 (23.4-176.6)	n= 79 67.7 ± 26.4 (24.6-169.5)	n= 27 65.1 ± 39.0 (22.6-218.2)	n= 49 68.6 ± 22.0 (36.3-145.3)	n= 25 60.9 ± 24.1 (21.3-111.1)	n= 107 84.2 ± 27.7 (36.5-188.3)	< 0.009 ^c

MNCV= motor nerve conduction velocity; CMTNS= Charcot-Marie-Tooth Neuropathy Score; MC= Meissner corpuscles; IME= intrapapillary myelinated endings; NS= not significant; a data are expressed as mean + standard deviation (range); b ANOVA analysis with the Bonferroni post hoc test; c two-group comparison by using Mann-Whitney U-test.

Table 8. Clinical features of CMT2E patients.

Patients	III.1	III.2	III.3	III.4	III.5	IV.1	IV.2	IV.3	IV.4
Age at examination/sex	57/F	53/M	58/F	56/M	50/M	25/M	24/F	33/M	24/M
Onset age/symptoms	Adolescence/ Unsteady ankles	Childhood/ Toe walker	Adolescence/ Pes cavus	Childhood/ Unsteady ankles	Childhood/ Unsteady ankles	Childhood/ Toe walker	Childhood/ Balance	Childhood/ Toe walker	Childhood/ Unsteady ankles
Distal/Proximal weakness UL	(4-; 2; 4-)/-	(1; 1; 1)/ (4+; 4+; 5)	(4; 2; 4)/-	(1; 2; 1)/-	(1; 1; 1)/-	(2; 3; 2)/-	(5; 5; 4-)/-	(4-; 3; 4-)/-	(3; 4-; 3)/-
Distal/Proximal weakness LL	(4; 5)/-	(0; 0)/-	(4+; 5)/-	(0; 1)/ (3; 5)	(1; 1)/-	(4; 5)/-	-/-	(4-; 4)/-	(4-; 5)/-
Ankle deep tendon reflexes	Reduced	Absent	Absent	Absent	Absent	Absent	Normal	Absent	Absent
Joint position sense UL/LL	Normal/ Normal	Normal/ Toe	Normal/ Toe	Normal/ Toe	Normal/ Toe	Normal/ Normal	Normal/ Normal	Normal/ Normal	Normal/ Toe
Vibration sense UL/LL	Normal/ Knee	Normal/ Knee	Fingers/ Knee	Elbow/ Knee	Normal/ Knee	Elbow/ Knee	Normal/ Normal	Normal/ Normal	Normal/ Knee
Pinprick UL/LL	Normal/ Toe	Normal/ Ankle	Normal/ Toe	Wrist/ Knee	Normal/ Toe	Normal/ Toe	Normal/ Normal	Wrist/ Ankle	Normal/ Ankle
Light touch UL/LL	Normal/ Normal	Normal/ Ankle	Normal/ Ankle	Normal/ Ankle	Normal/ Normal	Normal/ Toe	Normal/ Normal	Normal/ Normal	Normal/ Ankle
Ulnar MNCV (CMAP)	40 m/s (3.1 mV)	NR	40 m/s (3.6 mV)	NR	37.3 m/s (1.5 mV)	27 m/s (2.3 mV)	41 m/s (9.5 mV)	36.6 m/s (7.7 mV)	39 m/s (3.2 mV)
CMTNS (phenotype)	16 (moderate)	30 (severe)	20 (moderate)	30 (severe)	23 (severe)	18 (moderate)	5 (mild)	15 (moderate)	17 (moderate)

Abbreviations: UL= upper limbs; LL= lower limbs; MNCV= motor nerve conduction velocity; CMAP= compound muscular action potential; CMTNS= Charcot-Marie-Tooth neuropathy score; NR= no response; – = weakness absent.

Motor weakness based on Medical Research Council Scale: upper limb distal weakness assessed by first dorsal interosseous, abductor pollicis brevis and adductor digiti minimi; upper limb proximal weakness assessed by deltoids, biceps brachii and triceps. Lower limb distal weakness assessed by anterior tibialis and gastrocnemius; lower limb proximal weakness assessed by iliopsoas and quadriceps. Numbers are based on the side that gave the worst score. For sensory examination: normal is no decrease compared to the examiner; the level given is the highest level where a deficit was detected.

Figure 1. A. Wasting of distal muscles in lower limbs leading to inverted champagne bottle legs. B. Example of wasting of intrinsic muscles of the hands. C. Pes cavus with hammer toes.



Figure 2. Schematic drawing of a neuron, its axon and Schwann cells with the major genes associated with Charcot-Marie-Tooth disease represented with their respective function and cellular compartment. Adapted from Saporta MA, Shy ME. Inherited peripheral neuropathies. *Neurol Clin* 2013;31:597-619; with permission.

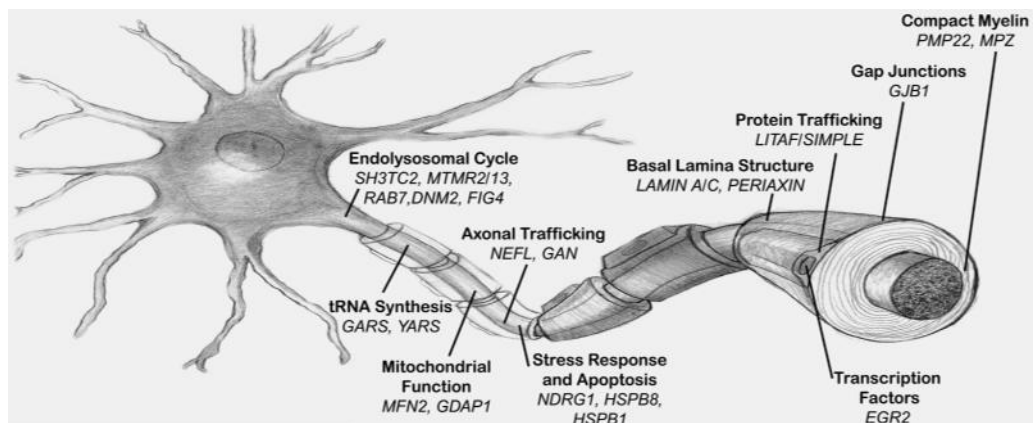


Figure 3. Pathologic findings in demyelinating Charcot-Marie-Tooth disease. A. Cross section of a sural nerve biopsy of a patient with demyelinating CMT showing numerous demyelinated axons (arrows) and occasional classical onion bulbs (asterisk). Thionine and acridine orange stain. Bar = 10 μ m. B. Electron micrograph showing a demyelinated axon (asterisk) surrounded by some excess basal lamina. The Schwann cells associated with small, unmyelinated axons are abnormally long and attenuated (arrows). Bar = 1 μ m. Adapted from Saporta MA, Shy ME. Peripheral neuropathies; with permission.

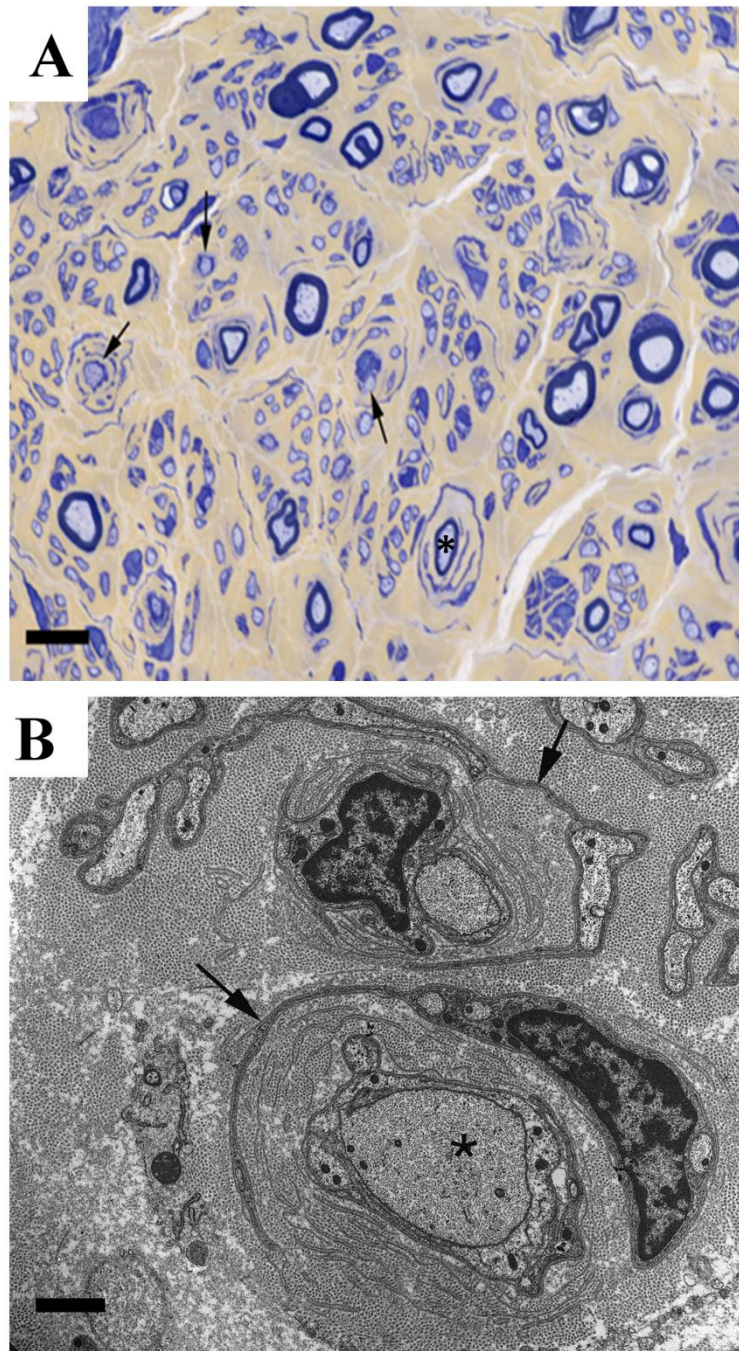


Figure 4. Pedigree of the CMT2E family.

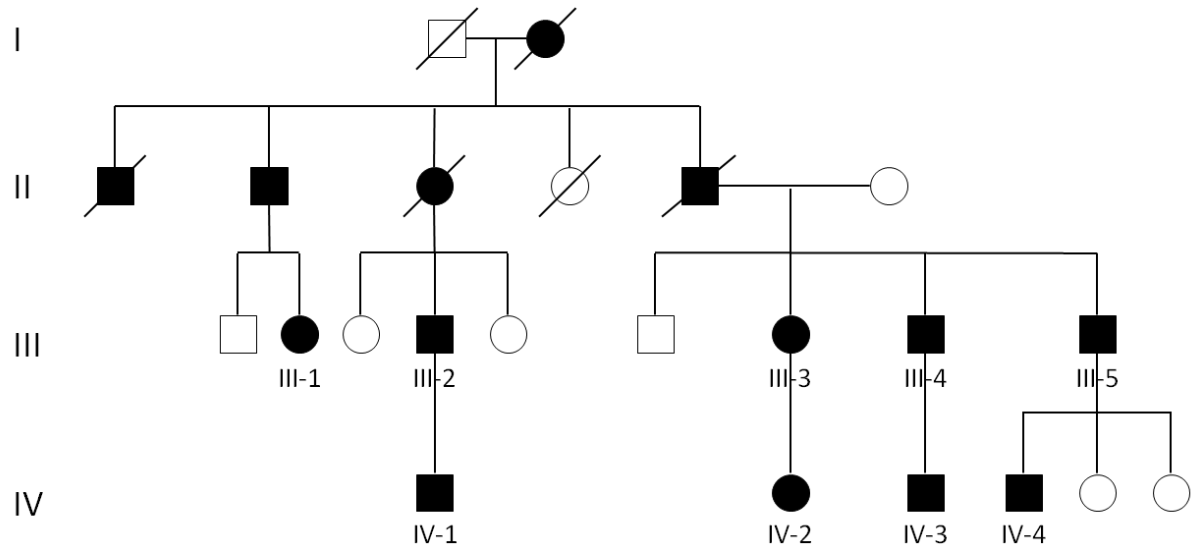


Figure 5. Confocal images showing morphometric analysis methods. In A and B: PGP/MBP double-stained images exemplifying the procedures used to measure node (B_2), internode (B_3) and fiber diameter (B_4) calculated as the mean value of four random measures along the internode. Measurements were performed on MBP channel as showed by arrowheads while PGP staining (arrow in B1) was necessary to check on axonal continuity. In C the nodal region on an image double stained with NF and MBP: branching originates always from nodes (arrowhead). In D₁ and D₂ the same image at higher magnification after splitting the two channels. Scale bar: 50 μm (A); 100 μm (C).

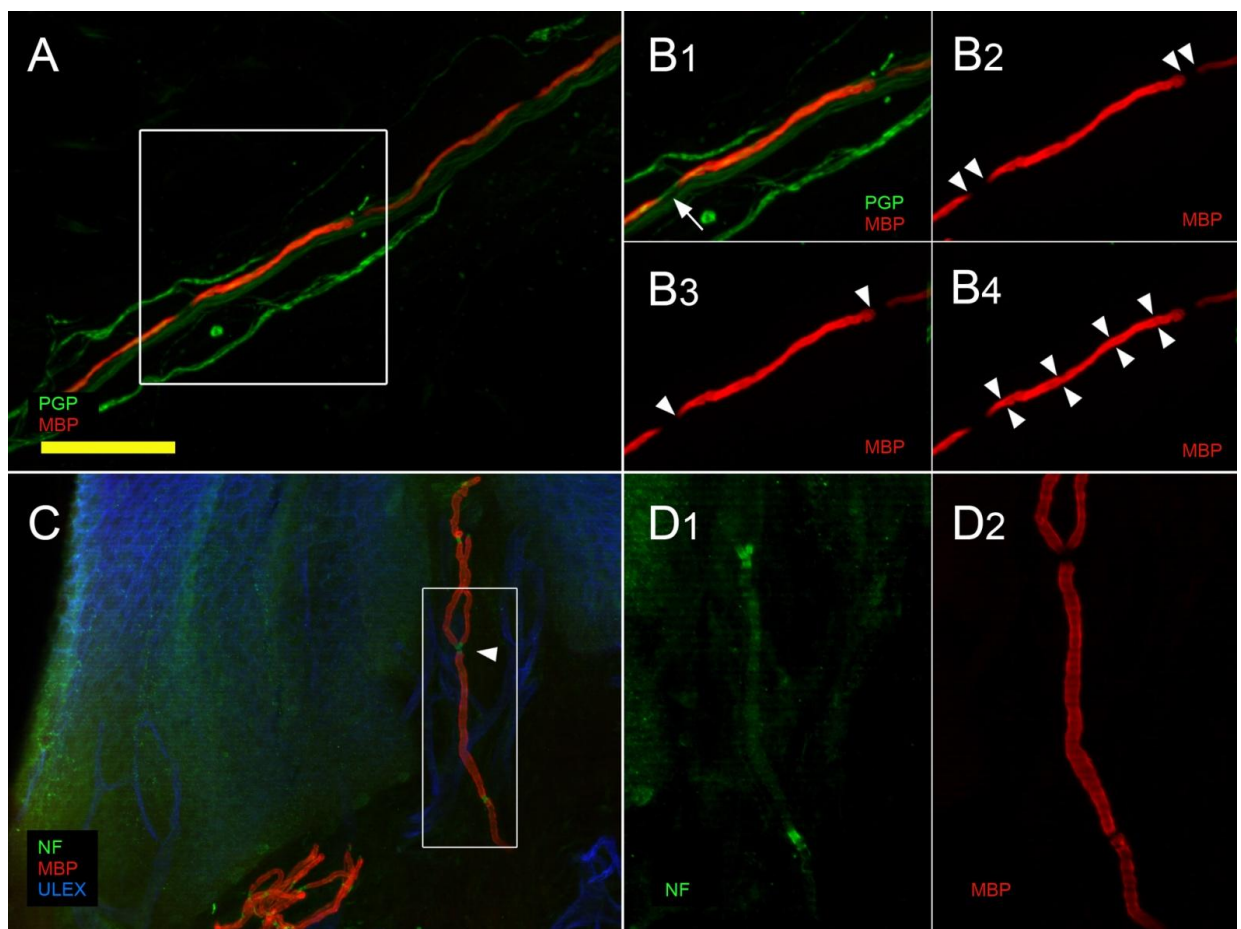


Figure 6. Somatic denervation in glabrous and hairy skin of CMT1A patient.

Digital images from fingertip (A, B), thigh (C, D) and leg (E, F) show epidermal and dermal denervation in patients with CMT1A. A moderate length-dependent loss of epidermal nerve fibers is present in patients with CMT1A compared to controls (B, D, F compared to A, C, E). Morphological abnormalities (arrowhead) and loss of Meissner corpuscles and intrapapillary myelinated endings are also evident in B. In addition to degenerative signs, frequent aspects of nerve remodeling (clusters) are observed (arrowheads in D and F). Scale bar: 100 μ m. COLIV= collagen IV; MBP= myelin basic protein; PGP= protein gene product.

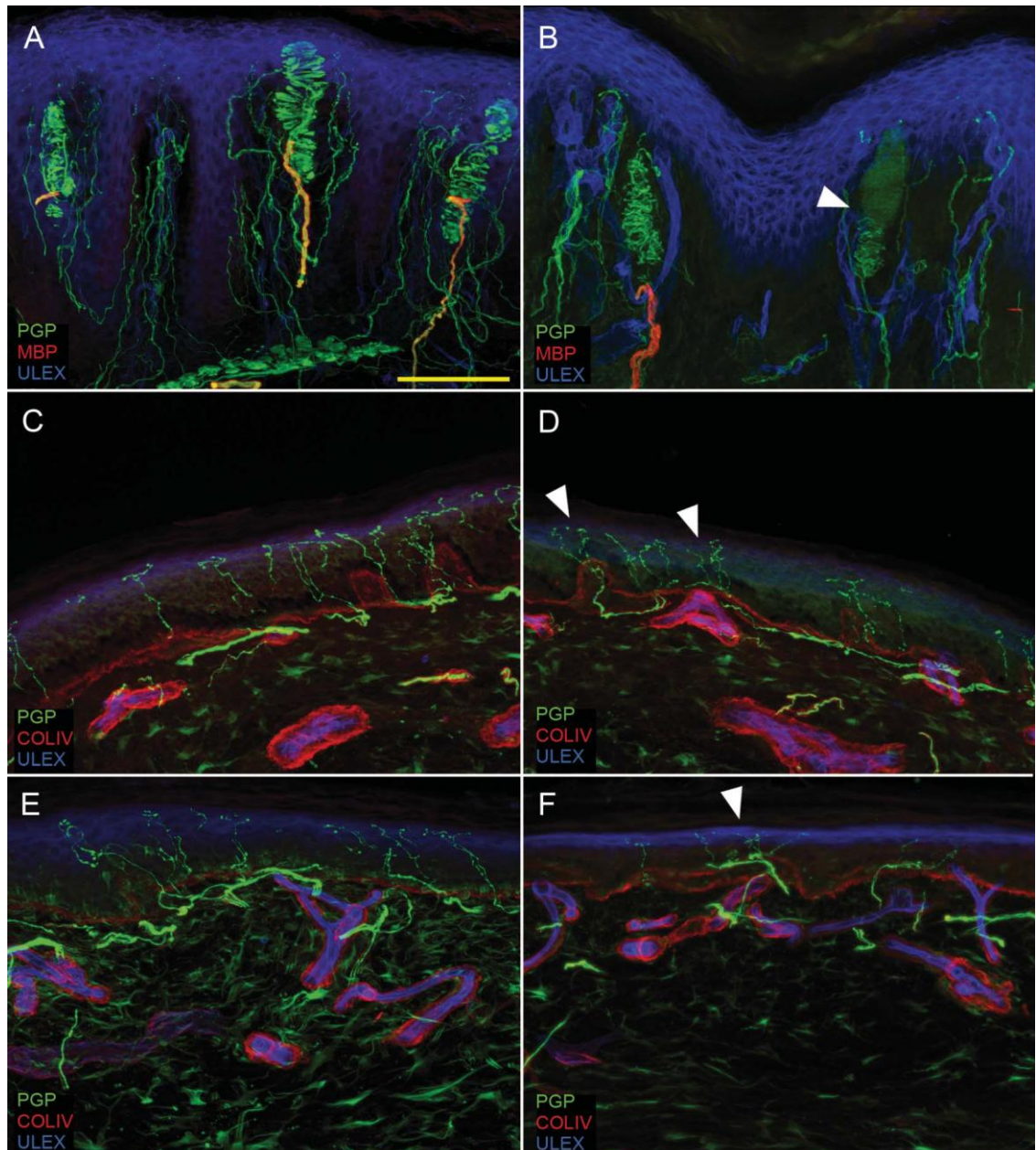


Figure 7. Cutaneous autonomic denervation in CMT1A patient.

Confocal images show, in patients compared to controls, loss of cholinergic sudomotor nerves (B compared to A), and loss of cholinergic and noradrenergic fibers in arteriovenous anastomoses (D compared to C) and arrector pili muscle (F compared to E). Scale bar: 100 μ m. VIP= vasoactive intestinal peptide; D β H= dopamine- β -hydroxylase.

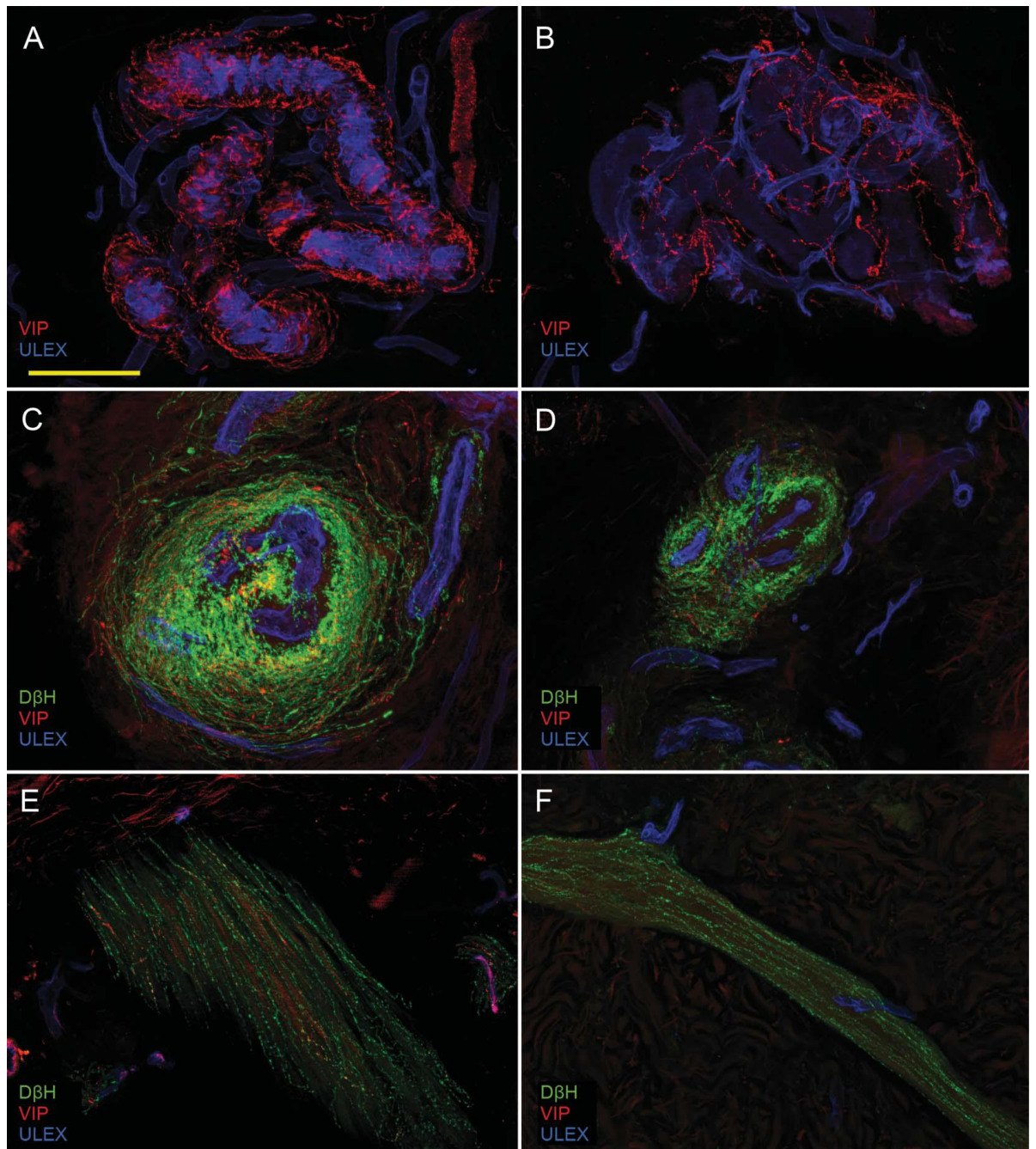


Figure 8. (A) Correlation between density of sudomotor nerve fibers and activated glands in CMT1A patient. (B) Age effect on ENF density.

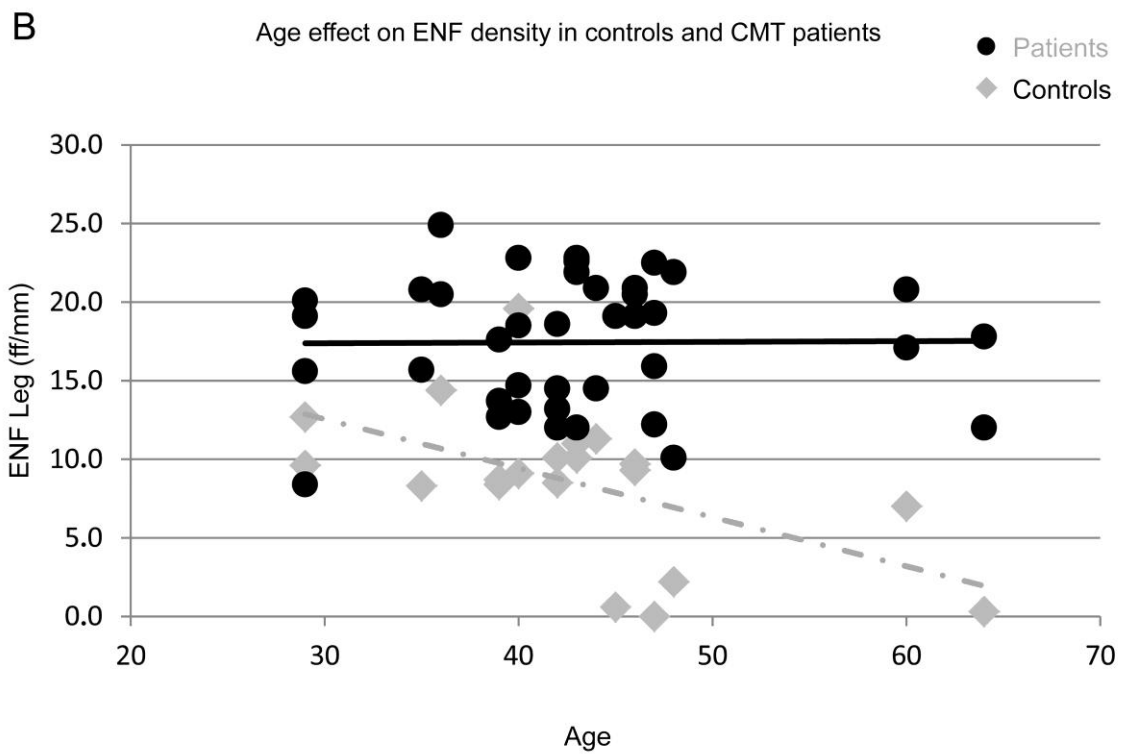
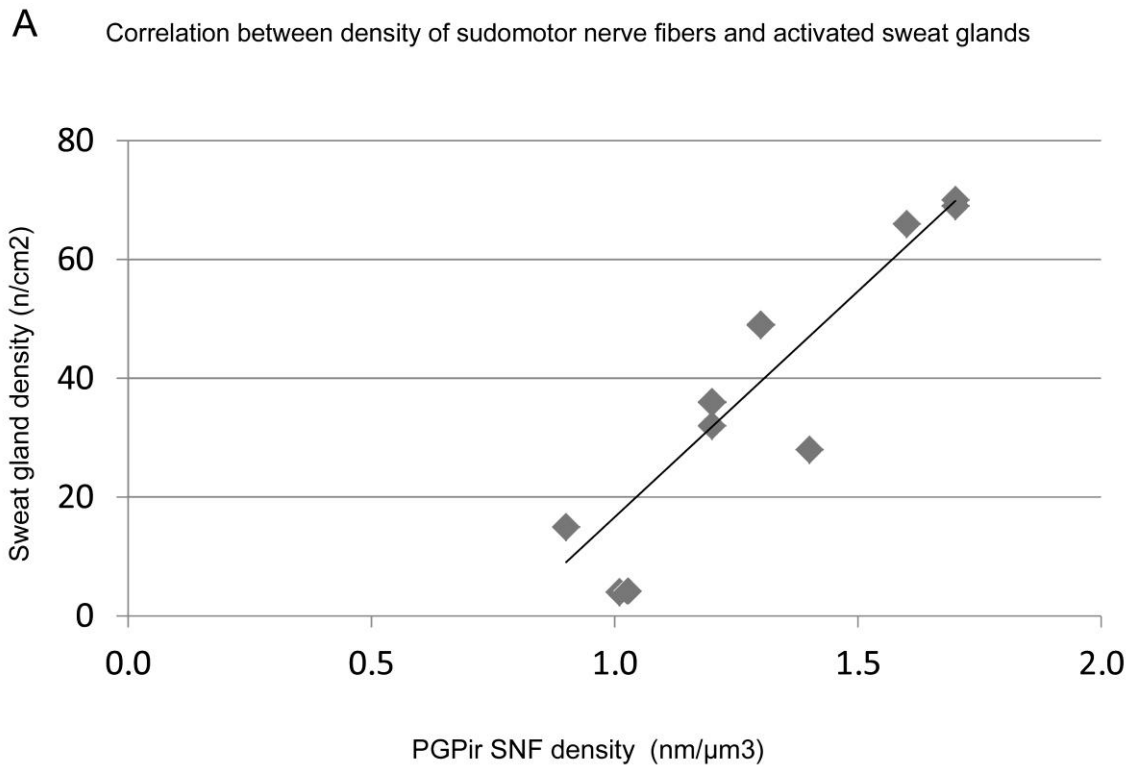


Figure 9. Confocal images of glabrous skin in CMT patients and controls. A moderate loss of Meissner corpuscles is observed in a patient with CMT1A (B) and a severe loss of Meissner corpuscles is present in a patient with RAB7 mutation (C), compared to a control (A). From D to F: abnormalities of myelinated fibers such as fragmentation (D) and swellings (arrowheads in E and F). G to I: disruption of nodal/paranodal architecture with elongation and asymmetry of the paranodes with expansion of neurofascin aggregation along the internode (arrows in H and I) compared to control (G). Scale bar: 200 μ m (A, B, C); 30 μ m (D, E, F); 50 μ m (G, H, I).

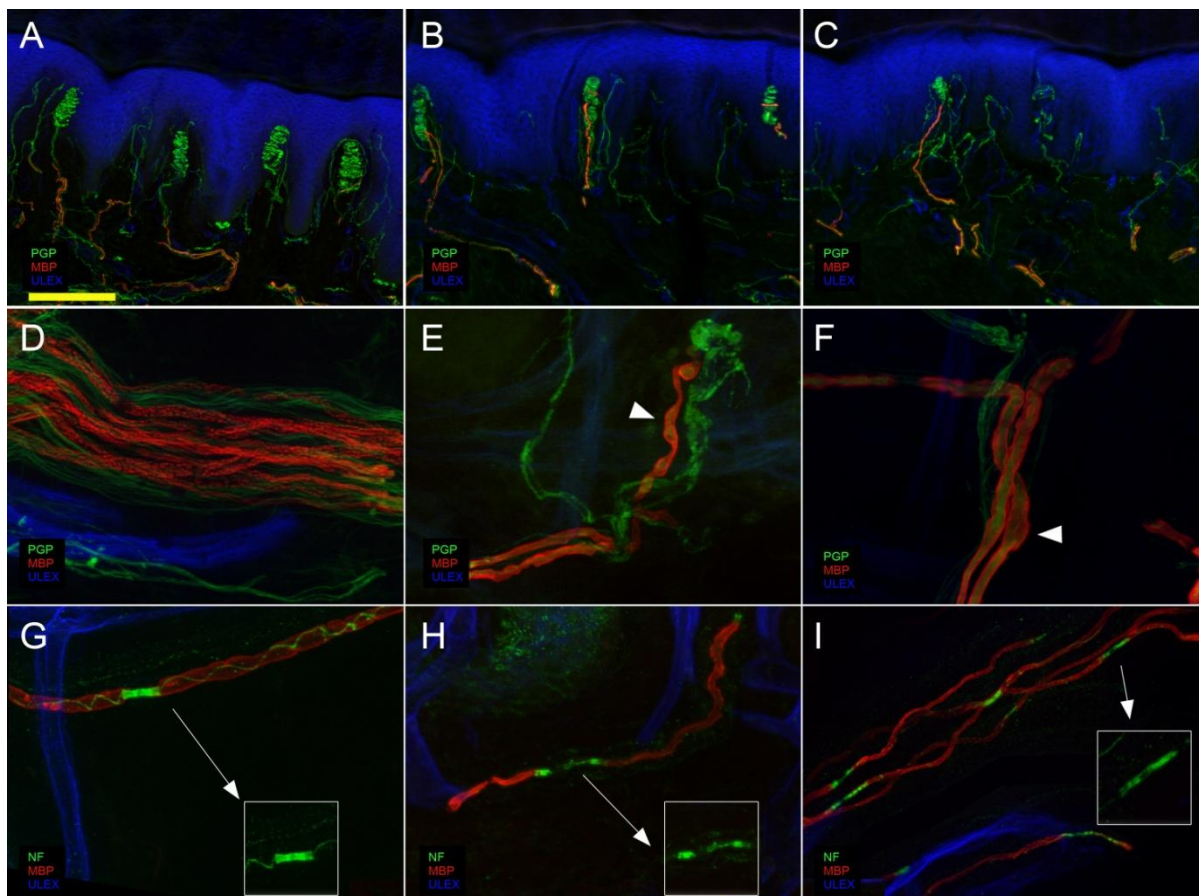


Figure 10. Boxplots of internodal length in each CMT genotype and controls. Dark horizontal lines represent the median value, with the box representing the 25th and 75th percentiles, the whiskers the lower and upper adjacent values, and outside values represented by dots.

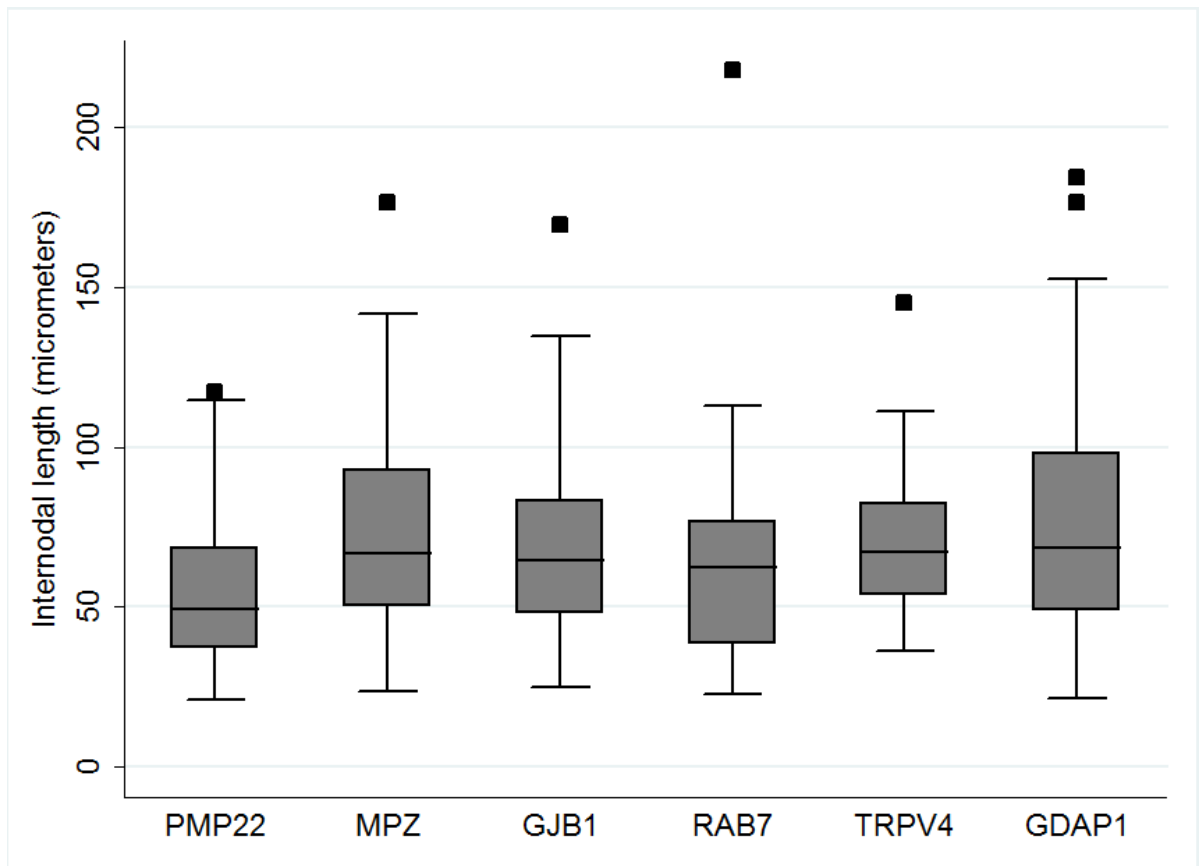


Figure 11. Cutaneous nerve fibers from CMT2E patients show a lack of NF.

(A) Confocal images of dermal axons stained with antibodies against PGP 9.5 (red), NF-L (green) and MBP (blue) in patient (IV, V) and control (I, II). A reduced or absent expression of NF is observed in patient compared to control. Confocal images of dermal nerve fibers stained with antibodies against α -tubulin (red), NF-L (green) and PGP 9.5 (blue) in patient (VI) and control (III). No difference in the expression of α -tubulin is found but a reduced NF labelling is still present in patient compared to control. Scale bar: 20 μ m. (B) Neurofilament (NF) fluorescence intensity (expressed as the percentage of the value of NF over the PGP intensity: NF/PGP ratio) between patients and controls. The ratio is significantly lower in each patient with respect to the controls ($p < 0.01$). (C) Western blot analysis of NF-L from skin of patients and control, normalized for α -tubulin. NF-L expression is decreased in patients with a complete absence of NF-L band in two of them, while α -tubulin expression is normal. (D) NF-L/ α -tubulin ratio is markedly reduced in patients compared to controls.

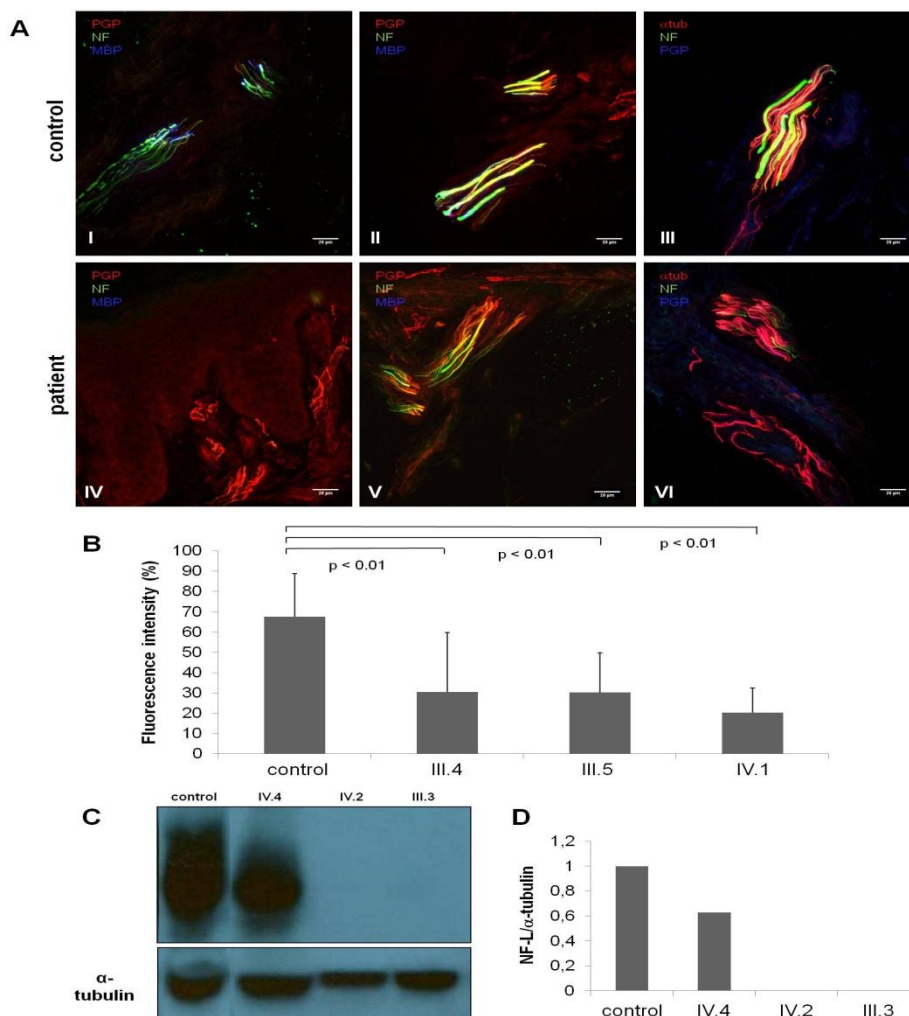


Figure 12. Electron microscopy images of dermal nerves in CMT2E (A).

Morphometric analysis of axonal caliber (B). (A) Electron microscopy images of dermal axons in CMT2E patient. Arrowheads: myelinated axons; arrow: unmyelinated axons; asterisk: Schwann cells without axons (bands of Bungner). No NF aggregates were detected. Scale bar: 2 μm . (B) Morphometric analysis showed smaller axonal calibers in patients than in controls ($p < 0.01$).

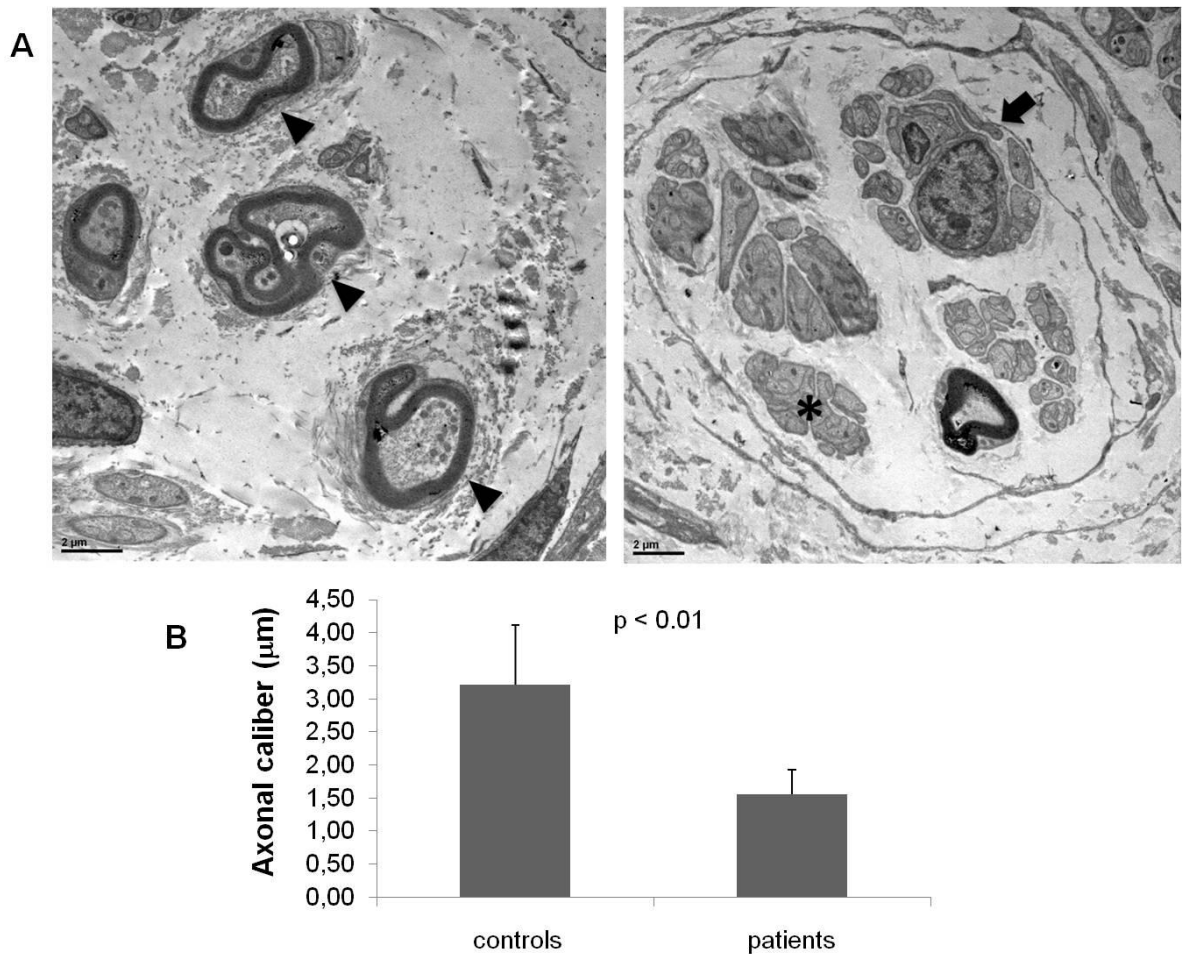
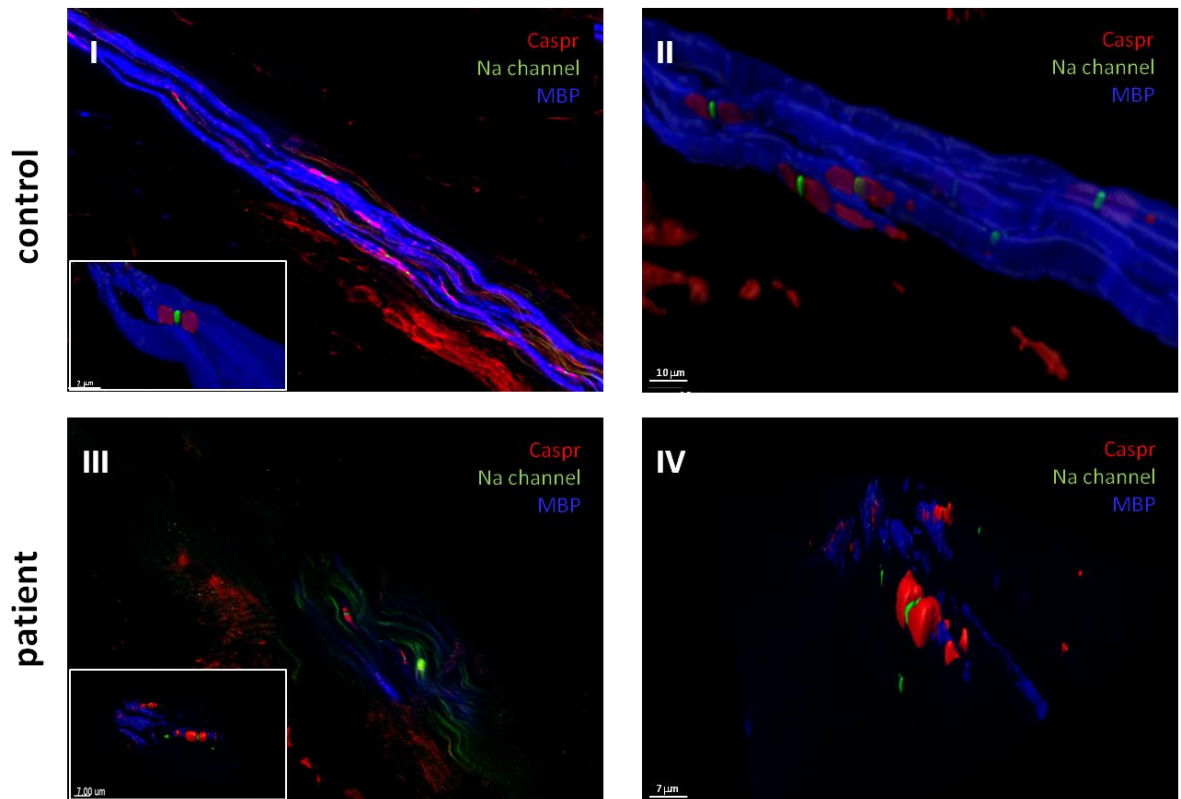


Figure 13. Nodal/paranodal architecture of dermal nerves. Confocal images of dermal axons stained with antibodies against Caspr (red), sodium channels (green) and MBP (blue), show normal architecture of nodal and paranodal regions in both patient (III, IV) and control (I, II). Scale bar: 20µm. Panel IV and the two small left corner figures in the panels I and III are 3D images of single or few nodes of Ranvier at higher magnification.



INDEX

1. INTRODUCTION	2
1.1 Charcot-Marie-Tooth disease	2
• <i>Epidemiology</i>	2
• <i>Clinical Manifestations</i>	3
• <i>Electrophysiology</i>	4
• <i>Pathobiology</i>	4
2. BACKGROUND	
2.1 CMT and skin biopsy	6
2.2 Axonal degeneration in CMT	7
3. AIM OF THE STUDY	8
4. MATERIALS AND METHODS	8
4.1 Patients	8
4.2 Skin biopsy	9
• <i>Immunofluorescence</i>	9
– <u><i>Quantification of cutaneous nerves – Somatic nerves</i></u>	9
– <u><i>Quantification of cutaneous nerves – Autonomic nerves</i></u>	10
– <u><i>Morphometric analysis of myelinated nerve fibers</i></u>	10
– <u><i>Fluorescence quantification</i></u>	11
• <i>Electron microscopy</i>	11
• <i>Western blot analysis</i>	12
4.3 Functional studies	12
• <i>Small Fiber Neuropathy Symptoms Inventory Questionnaire</i>	12
• <i>Quantitative Sensory Testing</i>	13
• <i>Dymanic Sweat Test</i>	13
• <i>Sympathetic Skin Response</i>	13
• <i>Cardiovascular Reflexes</i>	14
4.4 Statistical analysis	14
5. RESULTS	14
5.1 Patients	14
5.2 Small fiber involvement in CMT1A	14
• <i>Skin biopsy findings</i>	14
• <i>Functional studies</i>	15
5.3 Large fiber investigation in different CMT subtypes	16
• <i>Morphological analysis</i>	16
• <i>Morphometric analysis</i>	17
5.4 Study of the axonal transport proteins in CMT2E	17
• <i>Immunofluorescence and Western blot analysis</i>	17
• <i>Electron microscopy</i>	18
• <i>Morphometric analysis</i>	18
• <i>Study of nodal and paranodal region</i>	19
6 DISCUSSION	19

6.1 Small fiber involvement in CMT1A	19
• <i>Somatic nerves</i>	19
• <i>Autonomic nerves</i>	21
6.2 Large fiber involvement in different CMT subtypes	22
• <i>Axonal loss</i>	22
• <i>Nodal gap length</i>	23
• <i>Internodal length</i>	24
• <i>Effects of nodal and internodal length on nerve conduction velocity</i>	24
6.3 Reduced neurofilament expression in cutaneous nerve fibers of patients with CMT2E	25
7 CONCLUSIONS	27
8 REFERENCES	28
9 TABLES	38
10 FIGURES	47